Title

15-Lipoxygenase-1 biosynthesis of 7S,14S-diHDHA implicates 15-lipoxygenase-2 in biosynthesis of resolvin D5.

Journal

Journal of lipid research, 61(7)

ISSN

0022-2275

Authors

Perry, Steven C
Kalyanaraman, Chakrapani
Tourdot, Benjamin E
et al.

Publication Date

2020-07-01

DOI

10.1194/jlr.ra120000777

Peer reviewed

15-Lipoxygenase-1 biosynthesis of 7S,14S-diHDHA implicates 15-lipoxygenase-2 in biosynthesis of resolvin D5[S]

Steven C. Perry,* Chakrapani Kalyanaraman,† Benjamin E. Tourdot,§ William S. Conrad,* Oluwayomi Akinkugbe,* John Cody Freedman,* Michael Holinstat,§ Matthew P. Jacobson,† and Theodore R. Holman[1,*]

Department of Chemistry and Biochemistry,* University of California Santa Cruz, Santa Cruz, CA 95064; Department of Pharmaceutical Chemistry,† School of Pharmacy, University of California San Francisco, San Francisco, CA 94143; and Department of Pharmacology,§ University of Michigan Medical School, Ann Arbor, MI 48109

ORCID ID: 0000-0001-8072-2959 (T.R.H.)

Abstract The two oxylipins 7S,14S-dihydroxydocosahexaenoic acid (diHDHA) and 7S,17S-diHDHA [resolvin D5 (RvD5)] have been found in macrophages and infectious inflammatory exudates and are believed to function as specialized pro-resolving mediators (SPMs). Their biosynthesis is thought to proceed through sequential oxidations of DHA by lipoxygenase (LOX) enzymes, specifically, by human 5-LOX (h5-LOX) first to 7(S)-hydroxy-4Z,8E,10Z,13Z,16Z,19Z-DHA (7S-HDHA), followed by human platelet 12-LOX (h12-LOX) to form 7(S),14(S)-dihydroxy-4Z,8E,10Z,12E,16Z,19Z-DHA (7S,14S-diHDHA) or human reticulocyte 15-LOX-1 (h15-LOX-1) to form RvD5. In this work, we determined that oxidation of 7(S)-hydroperoxy-4Z,8E,10Z,13Z,16Z,19Z-DHA to 7S,14S-diHDHA is performed with similar kinetics by either h12-LOX or h15-LOX-1. The oxidation at C14 of DHA by h12-LOX was expected, but the noncanonical reaction of h15-LOX-1 to make over 80% 7S,14S-diHDHA was larger than expected. Results of computer modeling suggested that the alcohol on C7 of 7S-HDHA hydrogen bonds with the backbone carbonyl of Ile399, forcing the hydrogen abstraction from C12 to oxygenate on C14 but not C17. This result raised questions regarding the synthesis of RvD5. Strikingly, we found that h15-LOX-2 oxygenates 7S-HDHA almost exclusively at C17, forming RvD5 with faster kinetics than does h15-LOX-1. The presence of h15-LOX-2 in neutrophils and macrophages suggests that it may have a greater role in biosynthesizing SPMs than previously thought. We also determined that the reactions of h5-LOX with 14(S)-hydroperoxy-4Z,7Z,10Z,12E,16Z,19Z-DHA and 17(S)-hydroperoxy-4Z,7Z,10Z,13Z,15E,19Z-DHA are kinetically slow compared with DHA, suggesting that these reactions may be minor biosynthetic routes in vivo. Additionally, we show that 7S,14S-diHDHA and RvD5 have anti-aggregation properties with platelets at low micromolar potencies, which could directly regulate clot resolution.—Perry, S. C., C. Kalyanaraman, B. E. Tourdot, W. S. Conrad, O. Akinkugbe, J. C. Freedman, M. Holinstat, M. P. Jacobson, and T. R. Holman. **15-Lipoxygenase-1 biosynthesis of 7S,14S-diHDHA implicates 15-lipoxygenase-2 in biosynthesis of resolvin D5. *J. Lipid Res.* 2020.** 61: **1087–1103.**

Supplementary key words kinetics • docosahexaenoic acid • maresin • molecular modeling • platelets • mass spectrometry • enzymology • omega-3 fatty acid • human reticulocyte 15-lipoxygenase-1 • 7-hydroxydocosahexaenoic acid • 7(S),14(S)-dihydroxy-4Z,8E,10Z,12E,16Z,19Z-docosahexaenoic acid

Inflammation plays an essential role in the body, and in its acute form, it involves the upregulation of localized

Abbreviations: DGLA, dihomo-gamma-linoleic acid; 7-epi-MaR1, 7(S),14(S)-dihydroxy-4Z,8E,10E,12Z,16Z,19Z-DHA; FLAP, 5-lipoxygenase-activating protein; GLA, gamma-linoleic acid; h5-LOX, human 5-lipoxygenase; h12-LOX, human platelet 12-lipoxygenase; h15-LOX-1, human reticulocyte 15-lipoxygenase-1; h15-LOX-2, human epithelial 15-lipoxygenase-2; LOX, lipoxygenase; MaR1, 7(R),14(S)-dihydroxy-4Z,8E,10E,12Z,16Z,19Z-DHA; PDB, Protein Data Bank; RvD5, resolvin D5; 7S-HDHA, 7(S)-hydroxy-4Z,8E,10Z,13Z,16Z,19Z-DHA; 14S-HDHA, 14(S)-hydroxy-4Z,7Z,10Z,12E,16Z,19Z-DHA; 17S-HDHA, 17(S)-hydroxy-4Z,7Z,10Z,13Z,15E,19Z-DHA; 5S-HETE, 5(S)-hydroxy-6E,8Z,11Z,14Z-eicosatetraenoic acid; 12S-HETrE, 12(S)-8Z,10E,14Z-hydroxy-eicosatrienoic acid; 7S-HpDHA, 7(S)-hydroperoxy-4Z,8E,10Z,13Z,16Z,19Z-DHA; 8-HpDHA, 8(S)-hydroperoxy-4Z,6E,10Z,13Z,16Z,19Z-DHA; 11-HpDHA; 11(S)-hydroperoxy-4Z,7Z,9E,13Z,16Z,19Z-DHA; 16-HpDHA; 16(S)-hydroperoxy-4Z,7Z,10Z,13Z,17E,19Z-DHA; 14S-HpDHA, 14(S)-hydroperoxy-4Z,7Z,10Z,12E,16Z,19Z-DHA; 17S-HpDHA, 17(S)-hydroperoxy-4Z,7Z,10Z,13Z,15E,19Z-DHA; 20-HpDHA; 20(S)-hydroperoxy-4Z,7Z,10Z,13Z,16Z,18E-DHA; 12S-HpETE, 12(S)-hydroperoxy-5Z,8Z,10E,14Z-eicosatetraenoic acid; 7S,14S-diHDHA, 7(S),14(S)-dihydroxy-4Z,8E,10Z,12E,16Z,19Z-DHA; 7S,17S-diHDHA, 7(S),17(S)-dihydroxy-4Z,8E,10Z,13Z,15E,19Z-DHA; 7S,14S-diHpDHA, 7(S),14(S)-dihydroperoxy-4Z,8E,10Z,12E,16Z,19Z-DHA; 7S,17S-diHpHA, 7(S),17(S)-dihydroperoxy-4Z,8E,10Z,13Z,15E,19Z-DHA; SPM, specialized pro-resolving mediator.

[1] To whom correspondence should be addressed.
e-mail: holman@ucsc.edu

[S] The online version of this article (available at https://www.jlr.org) contains a supplement.

This work was supported by National Institutes of Health Grants R01 GM105671 (M.H., T.R.H.), R01 HL11405 (M.H., T.R.H.), R35 GM131835 (M.H., T.R.H.), and K99 HL136784 (B.E.T.). The content is solely the responsibility of the authors and does not necessarily represent the official views of the National Institutes of Health. M.P.J. is a consultant to and shareholder of Schrodinger LLC, which licenses the software used in this work.

Manuscript received 24 March 2020 and in revised form 8 May 2020.

Published, JLR Papers in Press, May 13, 2020
DOI https://doi.org/10.1194/jlr.RA120000777

inflammatory signaling molecules and cytokines that attract neutrophils to an area of injury (1). Over time, an area of injury begins producing specialized pro-resolving mediators (SPMs), which actively downregulate the immune response (2), a process referred to as the resolution of inflammation. Misregulation of the transition to resolution can extend the early beneficial effects of acute inflammation into the damaging effects of chronic inflammation, as seen in cardiovascular disease (3–5), diabetes (6, 7), and autoimmune disorders (8).

SPMs are oxylipins produced by the oxygenation of fatty acids by cyclooxygenases, lipoxygenases (LOXs), and cytochrome P450s (9). LOXs catalyze the stereospecific peroxidation of PUFAs containing a bis-allylic carbon moiety (10). The two 15-LOX isozymes, human reticulocyte 15-LOX-1 (h15-LOX-1 or ALOX15), primarily expressed in reticulocytes and macrophages (11, 12), and human epithelial 15-LOX-2 (h15-LOX-2 or ALOX15b), expressed in macrophages, neutrophils, skin, hair roots, and prostate (3, 13, 14), are named for their ability to stereospecifically oxygenate at C15 of AA (10). h15-LOX-1 converts AA into a mixture of approximately 90% 15(S)-hydroperoxy-5Z,8Z,11Z,13E-eicosatetraenoic acid (15S-HpETE) and 10% 12(S)-hydroperoxy-5Z,8Z,10E,14Z-eicosatetraenoic acid (12S-HpETE), while h15-LOX-2 oxygenates substrates with strict regiospecificity (15), producing only 15-HpETE from AA. h15-LOX-1 is implicated in many diseases, such as inflammation, stroke, colorectal cancer, and atherosclerosis (11), while h15-LOX-2 has only recently been identified as playing a role in atherosclerosis and inflammation (4, 16).

Many SPMs are synthesized at sites of inflammation and maresin 1 [7(R),14(S)-dihydroxy-4Z,8E,10E,12Z,16Z,19Z-DHA (MaR1)], which is made from DHA (17), plays a role in the resolution of inflammation by reducing platelet aggregation (18), reducing neutrophil chemotaxis, and increasing phagocytosis in leukocytes (19). In conjunction with the detection of MaR1 in cell extracts, Serhan and coworkers discovered three analogs of MaR1, 7(S),14(S)-dihydroxy-4Z,8E,10E,12Z,16Z,19Z-DHA (7-epi-MaR1), 7(R),14(S)-dihydroxy-4Z,8E,10E,12E,16Z,19Z-DHA (i.e., *EEE*-MaR1), and 7(S),14(S)-dihydroxy-4Z,8E,10Z,12E,16Z,19Z-DHA (7S,14S-diHDHA) (**Fig. 1**) (17). These three analogs were shown to affect macrophage chemotaxis but were less potent than MaR1. In particular, 7S,14S-diHDHA appeared to be biosynthesized in a di-oxygenation fashion without an epoxide intermediate, distinct from the other analogs. Its structure suggests that it is synthesized through two sequential LOX oxygenation reactions at C7 and C14, without the requirement of a hydrolase to open the epoxide intermediate (20–22). Given these oxygenation sites, as well as the enzymatic preferences of specific LOX isozymes, it is reasonable to assume that the biosynthesis of 7S,14S-diHDHA involves human 5-LOX (h5-LOX) oxidizing DHA at C7, with human platelet 12-LOX (h12-LOX) oxidizing at C14, but it is unclear which oxidation occurs first (**Scheme 1**, pathway 2).

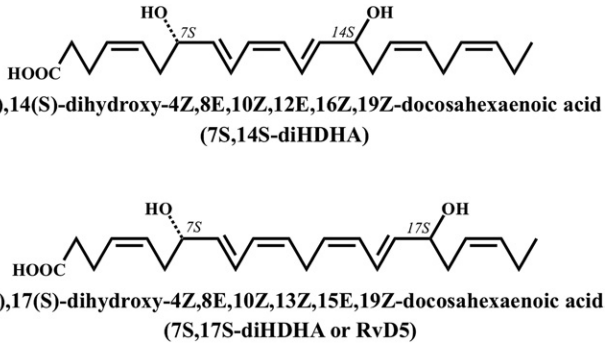

Fig. 1. Structures of 7S,14S-diHDHA and 7S,17S-diHDHA (or RvD5). Note that the molecules are drawn with an artificial straight chain shape in order to highlight their similarities and differences more clearly.

The other SPM, which is of importance with regard to this work, is resolvin D5 (RvD5) [or 7(S),17(S)-dihydroxy-4Z,8E,10Z,13Z,15E,19Z-DHA (7S,17S-diHDHA)] (Fig. 1). RvD5 is a D-series resolvin made from DHA (23, 24), which enhances phagocytosis in neutrophils and macrophages and reduces expression of the pro-inflammatory molecules, NF-κB and TNF-α (25), and has been identified in human blood, hemorrhagic exudates, and synovial fluid (26, 27). Like 7S,14S-diHDHA, the production of RvD5 appears to require two oxygenation events and is proposed to occur through the sequential reaction of two LOXs (27, 28). Because many cell types contain only a single LOX, oxylipins with multiple oxygenation sites are often created by the interaction of multiple cell types in an area of inflammation through a process called transcellular biosynthesis (29–31). RvD5 has been isolated from neutrophils (32) and is produced late in the process of blood coagulation, increasing over the lifetime of a clot (33). Polymorphonuclear leukocytes have been shown to convert 17(S)-hydroxy-4Z,7Z,10Z,13Z,15E,19Z-DHA (17S-HDHA) into 4(S),17(S)-dihydroxy-5E,7Z,10Z,13Z,15E,19Z-DHA (4S,17S-diHDHA) and RvD5 (27), suggesting that h5-LOX reacts with 17-HDHA to produce RvD5.

As stated above, LOX isozymes play a key role in the biosynthesis of SPMs; however, the biosynthetic molecular mechanism for specific SPMs is poorly defined. For 7S,14S-diHDHA, the current understanding of its biosynthetic pathway is based on the substrate specificity of h5-LOX and h12-LOX with AA and experimental evidence that the nonspecific LOX inhibitor, baicalein, reduces the production of MaR1 and 14(S)-dihydroxy-4Z,7Z,10Z,12E,16Z,19Z-DHA (14S-HDHA) (34). However, baicalein is not a selective inhibitor (35) and LOXs can produce different products depending on the fatty acids or oxylipin used (36–38). For example, h15-LOX-1 produces 41% of the noncanonical product, 14(S)-hydroperoxy-4Z,7Z,10Z,12E,16Z,19Z-DHA (14S-HpDHA), from DHA, which is proposed to be linked to human evolution and the human inflammatory response, with only higher primates having this LOX function (39). This ability of h15-LOX-1 to oxygenate either C17 or C14 on DHA raises the possibility that h15-LOX-1 could generate significant amounts of 7S,14S-diHDHA from DHA (40), as shown in Scheme 1, pathway 3.

For RvD5, the generally accepted biosynthetic pathway is through transcellular biosynthesis, but a specific biosynthetic

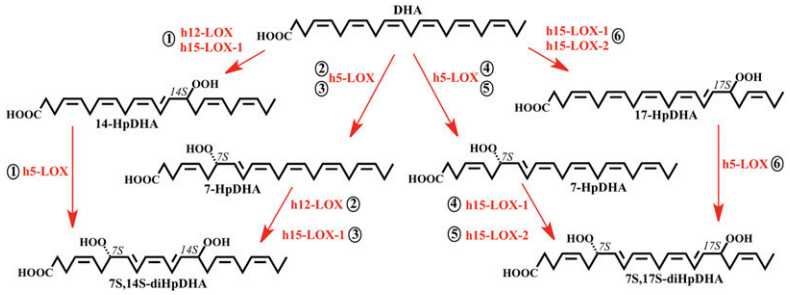

Scheme 1. The synthesis of 7S,14S-diHDHA from DHA may occur through one of three possible pathways: reaction of DHA with h5-LOX followed by h12-LOX (circled number 2), reaction of DHA with h5-LOX followed by h15-LOX-1 (circled number 3), or reaction of DHA with h12-LOX or h15LOX-1 followed by h5-LOX (circled number 1). The synthesis of RvD5 from DHA may also occur through three possible pathways: reaction of DHA with h5-LOX followed by h15-LOX-1 (circled number 4), reaction of DHA with h5-LOX followed by h15-LOX2 (circled number 5), or reaction of DHA with h12-LOX, h15-LOX-1, or h15LOX-2 followed by h5-LOX (circled number 6).

sequence has not been clearly identified. One proposed pathway is that h5-LOX, expressed in macrophages (41, 42) and polymorphonuclear leukocytes (27), produces 7(S)-hydroxy-4Z,8E,10Z,13Z,16Z,19Z-DHA (7S-HDHA) from DHA, and then h15-LOX-1 reacts with 7S-HDHA to produce RvD5 by oxidation at C17 (43). This is a reasonable assumption because h15-LOX-1 oxygenates C17 of DHA efficiently; however, because h15-LOX-1 also makes a significant amount of the C14 product and h15-LOX-2 is expressed at higher levels than h15-LOX-1 in both neutrophils and macrophages (4, 13, 44), it is possible that h15-LOX-2, and not h15-LOX-1, may be involved in the formation of RvD5 from 7S-HDHA (Scheme 1). It should be noted that LOXs produce the hydroperoxy product, but the reducing environment of the cell quickly reduces them to the hydroxy products (45), such as 7S,14S-diHDHA and 7S,17S-diHDHA (RvD5).

Given the biological importance of SPMs, such as 7S,14S-diHDHA and 7S,17S-diHDHA (RvD5), and the multiple possible biosynthetic pathways for their production, we investigated two critical aspects of the biosynthetic routes to producing these two SPMs: the ease of which LOXs can perform the proposed reactions in vitro (i.e., kinetics) and the specificity of LOXs when the substrate is an oxylipin, as opposed to an unoxidized fatty acid. We probed these effects in the production of both 7S,14S-diHDHA and 7S,17S-diHDHA (RvD5) and determined that not only are the rates greatly affected by the nature of the oxylipin substrate, but the product profile is also altered, raising the possibility that unrecognized noncanonical LOXs may be involved in SPM production.

MATERIALS AND METHODS

Expression and purification of h15-LOX-1, h15-LOX-2, h12-LOX, and h5-LOX

Overexpression and purification of WT h15-LOX-1 (UniProt entry P16050), h12-LOX (UniProt entry P18054), h5-LOX (UniProt entry P09917), and h15-LOX-2 (UniProt entry O15296) were performed as previously described (46–48). The purity of h12-LOX, h15-LOX-1, and h15-LOX-2 were assessed by SDS gel to be greater than 85% and metal content was assessed on a Finnigan inductively coupled plasma mass spectrometer, via comparison with iron standard solution. Cobalt-EDTA was used as an internal standard. The WT h5-LOX used in the kinetics of this work was not purified due to a dramatic loss in activity and was therefore prepared as an ammonium-sulfate precipitate. The amount of h5-LOX contained in the ammonium-sulfate pellet was assessed by comparing values obtained by a Bradford assay and quantitative Western blotting using purified stable-h5-LOX mutant as a positive control. Western blots were performed using rabbit anti-5-LOX polyclonal (Cayman Chemicals) primary antibody diluted 1:500 and goat anti-rabbit-HRP (Abcam) secondary antibody diluted 1:5,000. The stable-h5-LOX mutant was expressed in Rosetta 2 cells (Novagen) transformed with the pET14b-Stable-5-LOX plasmid (a gift from Marcia Newcomer of Louisiana State University) and grown in Terrific Broth containing 34 μg ml^{-1} chloramphenicol and 100 μg ml^{-1} ampicillin at 37°C for 3.5 h and then placed at 20°C for an additional 26 h. Cells were pelleted and resuspended in 50 mM Tris (pH 8.0), 500 mM NaCl, 20 mM imidazole with 1 μM pepstatin, 100 μM PMSF, and DNaseI (2 Kunitz/g) (Sigma). The cells were lysed in a French pressure cell and centrifuged at 40,000 *g* for 20 min. Lysate was applied to a Talon nickel-IDA Sepharose column and eluted with 50 mM Tris (pH 8.0), 500 mM NaCl, and 200 mM imidazole. The final product was stored at −80°C with 10% glycerol.

Production and isolation of oxylipins

7(S)-hydroperoxy-4Z,8E,10Z,13Z,16Z,19Z-DHA (7S-HpDHA) was synthesized by reaction of DHA (25–50 μM) with h5-LOX. The reaction was carried out for 2 h in 800 ml of 25 mM HEPES (pH 7.5) containing 50 mM NaCl, 100 μM EDTA, and 200 μM ATP. The reaction was quenched with 0.5% glacial acetic acid, extracted three times with 1/3 vol dichloromethane, and evaporated to dryness under N_2. The products were purified isocratically via HPLC on a Higgins Haisil semi-preparative (5 μm, 250 × 10 mm) C18 column with 50:50 of 99.9% acetonitrile, 0.1% acetic acid and 99.9% water, 0.1% acetic acid. 7S-HDHA was synthesized as performed for 7S-HpDHA with trimethyl phosphite added as a reductant prior to HPLC. 7S,14S-diHDHA was synthesized by reaction of 20 μM 7S-HDHA with h15-LOX-1 in 300 ml of 25 mM HEPES (pH 7.5) and purified as described above. 14S-HpDHA was synthesized by reaction of DHA (25–50 μM) with h12-LOX. The reaction was carried out for 30 min in 1,000 ml of 25 mM HEPES (pH 8.0) The reaction was quenched with 0.5% glacial acetic acid, extracted three times with 1/3 vol dichloromethane, and evaporated to dryness under N_2. The products were purified isocratically via HPLC on a Phenomenex Luna semi-preparative (5 μm, 250 × 10 mm) silica column with 99:1 of 99.9% hexane,

0.1% trifluoroacetic acid and 99.9% isopropanol, 0.1% trifluoroacetic acid. 14S-HDHA was synthesized as performed for 14S-HpDHA with trimethyl phosphite added as a reductant prior to HPLC. 17(S)-hydroperoxy-4Z,7Z,10Z,13Z,15E,19Z-DHA (17S-HpDHA) was synthesized by reaction of DHA (25–50 μM) with soybean 15-LOX. The reaction was carried out for 1 h in 800 ml of 100 mM borate (pH 9.0). 17S-HDHA was synthesized by reducing 17S-HpDHA with trimethyl phosphite prior to HPLC. 7(S),17(S)-dihydroxydocosahexaenoic acid (7S,17S-diHDHA or RvD5) was synthesized by reacting 7S-HDHA (20 μM) with h15-LOX-2 in 300 ml of 25 mM HEPES (pH 7.5), with subsequent reduction/purification, as described above. The isolated products were assessed to be greater than 95% pure by LC-MS/MS.

Steady state kinetics of h15-LOX-1 and h12-LOX with DHA, 7S-HDHA, and 7S-HpDHA

h15-LOX-1 reactions were performed at ambient temperature in a 1 cm^2 quartz cuvette containing 2 ml of 25 mM HEPES (pH 7.5) with substrate (DHA, 7S-HDHA, or 7S-HpDHA). DHA concentrations were varied from 0.25 to 10 μM, 7S-HDHA concentrations were varied from 0.3 to 15 μM, and 7S-HpDHA concentrations were varied from 0.3 to 20 μM. Concentration of DHA was determined by measuring the amount of 17S-HpDHA produced from complete reaction with soybean LOX-1. Concentrations of 7S-HDHA and 7S-HpDHA were determined by measuring the absorbance at 234 nm. Reactions were initiated by the addition ∼200 nM h15-LOX-1 and were monitored on a Perkin-Elmer Lambda 45 UV/VIS spectrophotometer. Product formation was determined by the increase in absorbance at 234 nm for 7S-HpDHA (ε_{234nm} = 25,000 M^{-1} cm^{-1}) and 270 nm for 7S,14S-diHDHA (ε_{270nm} = 40,000 M^{-1} cm^{-1}) (34, 49, 50). 7S,17S-diHDHA has a UV absorbance maximum of 245 nm; however, due to overlap with the substrate peak at 234 nm, formation of this product was measured at 254 nm using an extinction coefficient of 21,900 M^{-1} cm^{-1} to adjust for the decreased rate of absorbance change at this peak shoulder (20). KaleidaGraph (Synergy) was used to fit initial rates (at less than 20% turnover), as well as the second order derivatives (k_{cat}/K_M) to the Michaelis-Menten equation for the calculation of kinetic parameters. h12-LOX reactions were performed similarly as for h15-LOX-1 except that buffers were 25 mM HEPES (pH 8), and reactions were initiated by the addition ∼50 nM h12-LOX.

Steady state kinetics of h5-LOX with DHA, 14S-HDHA, 14S-HpDHA, 17S-HDHA, and 17S-HpDHA

All h5-LOX kinetic reactions were carried out in 25 mM HEPES (pH 7.5) containing 50 mM NaCl, 100 μM EDTA, and 200 μM ATP. Steady state kinetics of h5-LOX with DHA were determined as for h15-LOX-1. V_{max} assay of h5-LOX with 14S-HDHA, 14S-HpDHA, 17S-HDHA, and 17S-HpDHA were carried out in 15 ml of buffer containing 10 μM substrate. Reactions were initiated by the addition ∼600 nM ammonium-sulfate-precipitated h5-LOX and were monitored on a Perkin-Elmer Lambda 45 UV/VIS spectrophotometer. Reactions were quenched at 0, 5, 10, 20, 30, and 60 min. Each quenched reaction was extracted three times with 1/3 vol of DCM and reduced with trimethyl phosphite. The samples were then evaporated under a stream of N_2 to dryness and reconstituted in 90:10 acetonitrile:water containing 0.1% formic acid and 3 μM 13-HODE as an internal standard. Control reactions without enzyme were also conducted and used for background subtraction, ensuring that oxylipin degradation products were removed from analysis. Reactions were analyzed via LC-MS/MS using a Synergi 4 μM Hydro-RP 80 Å C18 LC-column with polar endcapping (150 × 2 mm). Mobile phase solvent A consisted of 99.9% water and 0.1% formic acid, and solvent B consisted of 99.9% acetonitrile and 0.1% formic acid. Analysis was carried out over 60 min using isocratic 50:50 A:B for 0–30 min followed by a gradient from 50:50 A:B to 75:25 A:B from 30 to 60 min. The chromatography system was coupled to a Thermo-Electron LTQ LC-MS/MS instrument for mass analysis. All analyses were performed in negative ionization mode at the normal resolution setting. MS/MS was performed in a targeted manner with a mass list containing the following *m/z* ratios (±0.5): 343.4 (HDHAs), 359.4 (diHDHAs), and 375.4 (triHDHAs). Products were identified by matching retention times, UV spectra, and fragmentation patterns to known standards, or in the cases were MS standards were not available, structures were deduced from comparison with known and theoretical fragments. MS/MS fragments used to identify 7,14-diHDHA included: 341, 297, 221, 177, 141, and 123. MS/MS fragments used to identify 7,17-diHDHA included: 341, 297, 261, 243, 199, and 141. MS/MS integrated peak areas were normalized to a 13-HODE internal standard and fitted to determine V_{max}. The catalytic activity relative to protein weight for h5-LOX was calculated by comparing V_{max} to protein concentration, which was determined by quantitative Western blotting, described above. For comparison of biosynthetic flux with h5-LOX, K_{cat} values for each enzyme and substrate were converted to V_{max} at 10 μM using the Michaelis-Menten equation and then multiplied by the percentage of total product represented by each reaction product.

Steady state kinetics of h15-LOX-2 with DHA, 7S-HDHA, and 7S-HpDHA

h15-LOX-2 reactions were performed at room temperature in a 1 cm^2 quartz cuvette containing 2 ml of 25 mM HEPES (pH 7.5) with substrate (DHA, 7S-HDHA, and 7S-HpDHA). DHA concentrations were varied from 0.75 to 50 μM; 7S-HDHA concentrations were varied from 0.6 to 30 μM; and 7S-HpDHA concentrations were varied from 0.6 to 25 μM. The concentration of DHA was determined by measuring the amount of 17S-HpDHA produced from complete reaction with soybean LOX-1 and confirmed by measuring turnover with h15-LOX-2. Concentrations of 7S-HDHA and 7S-HpDHA were determined by measuring absorbance at 234 nm. Reactions were initiated by the addition h15-LOX-2 (∼220 nM final concentration) and were monitored on a Perkin-Elmer Lambda 45 UV/VIS spectrophotometer. Product formation was determined by the change in absorbance at 234 nm for 7S-HDHA (ε_{234nm} = 25,000 M^{-1} cm^{-1}), 270 nm for 7S,14S-diHDHA (ε_{270nm} = 40,000 M^{-1} cm^{-1}), and 254 nm for 7S,17S-diHDHA (ε_{254nm} = 21,900 M^{-1} cm^{-1}) (20, 34, 49, 50). KaleidaGraph (Synergy) was used to fit initial rates (at less than 20% turnover) as well as the second order derivatives (k_{cat}/K_M) to the Michaelis-Menten equation for the calculation of kinetic parameters.

Product analysis of LOX reactions

Reactions were carried out in 2 ml of 25 mM HEPES (pH 7.5) with stirring at ambient temperature. Reactions with DHA and AA contained 10 μM substrate and ∼200 nM h15-LOX-1 and h15-LOX-2 in 2 ml of buffer. Those with h15-LOX-1 and 7S-HDHA, 7S-HpDHA, 14S-HDHA, and 14S-HpDHA contained 20 μM substrate and ∼600 nM of enzyme in 4 ml of buffer. Those with h15-LOX-2 and 7S-HDHA, 7S-HpDHA, 17S-HDHA, and 17S-HDHA contained 4 ml of buffer, 10 μM of substrate, and ∼450 nM of enzyme. The reaction of h5-LOX with DHA contained 10 μM substrate and ∼400 nM ammonium-sulfate-precipitated enzyme and was analyzed by LC-MS, as described above for h5-LOX kinetics. Reactions of h15-LOX-1, h15-LOX-2, and h12-LOX were analyzed by LC-MS as described above, with the exception that the LC gradient was carried out over 25 min using isocratic 40:60 A:B for 0–10 min followed by a gradient from 40:60 A:B to 75:25 A:B from 10 to 25 min. In order to minimize the formation of secondary products, reactions were quenched at less than 50% turnover. The presence of tri-HDHA secondary products was assessed by

monitoring at MS/MS filter of 359.4. Any tri-HDHAs observed were quantitated and included in the area of their respective parent di-HDHA.

Chiral chromatography

7S,14S-diHDHA and 7S,17S-diHDHA were synthesized by h15-LOX-1 and h15-LOX-2, respectively, and isolated via HPLC as described above. 7S,14S-diHDHA produced by h5-LOX was synthesized in 15 ml of buffer containing 10 μM 14S-HDHA and ~6 μM of ammonium-sulfate-precipitated h5-LOX. Purified 7S,14S-diHDHA and 7S,17S-diHDHA were analyzed via LC-MS/MS using a Chirapak AD-RH 2.1 × 150 mm, 5 μM chiral column coupled to a Thermo electron LTQ. Mobile phase solvent A consisted of 99.9% water, 0.1% formic acid and solvent B consisted of 99.9% acetonitrile, 0.1% formic acid. Analysis was carried out over 60 min using isocratic 35:65 A:B for 0–30 min followed by a gradient from 35:65 A:B to 75:25 A:B from 30 to 60 min. MS/MS conditions were the same as described above. Retention times and fragmentations were compared with RvD5, Mar1, and 7-epi-Mar standards purchased from Cayman Chemicals (Ann Arbor, MI).

Oxylipin titration into human platelets

The University of Michigan Institutional Review Board approved all research involving human volunteers. Washed platelets were isolated from human whole blood via serial centrifugation and adjusted to 3.0×10^8 platelets per milliliter in Tyrode's buffer (10 mM HEPES, 12 mM $NaHCO_3$, 127 mM NaCl, 5 mM KCl, 0.5 mM NaH_2PO_4, 1 mM $MgCl_2$, and 5 mM glucose), as previously published. Platelets (250 μl at 3.0×10^8 platelets per milliliter) were dispensed into glass cuvettes and incubated with the indicated oxylipin in half-log increments (0–10 μM) for 10 min at 37°C. Oxylipin-treated platelets were stimulated with 0.25 μg/ml of collagen (Chrono-log) under stirring conditions (1,100 rpm) at 37°C in a Chrono-log Model 700D lumi-aggregometer, and platelet aggregation was recorded for 6 min.

In order to determine whether 7S-HDHA was enzymatically converted to another chemical ex vivo, 1 ml of platelets (1.0×10^9 platelets per milliliter) was incubated with either 10 μM 7S-HDHA, 10 μM 5(S)-hydroxy-6E,8Z,11Z,14Z-eicosatetraenoic acid (5S-HETE) (positive control), or vehicle (DMSO) for 10 min at 37°C and then pelleted by centrifugation at 1,000 *g* for 2 min. Supernatant was transferred to a fresh tube and snap-frozen. Oxylipins were extracted and analyzed via UPLC-MS/MS, as described previously (9). The *m/z* transitions for 7S-HDHA, 7S,14S-diHDHA, 7S,17S-diHDHA were *m/z* 343.5→141, *m/z* 359.5→141, and *m/z* 359.5→199, respectively.

Molecular modeling

A structure of h15-LOX-1 (ALOX15) is not available in the Protein Data Bank (PDB). Therefore, we constructed a homology model of h15-LOX-1 from its sequence (UniProt entry P16050) using the substrate mimetic inhibitor-bound, high-resolution structure of porcine 12-LOX (PDB entry 3rde). The h15-LOX-1 sequence is 86% identical to the porcine 12-LOX sequence, with both being considered ALOX15 genes. The homology model was constructed using Prime software (version 5.4, Schrodinger Inc.). During the modeling step, we retained the cocrystallized inhibitor, metal ion (Fe^{3+}), and a hydroxide ion that coordinated the metal ion from the homolog structure. The model was subsequently energy minimized using the Protein Preparation Wizard module of Maestro (version 11.8, Schrodinger Inc). During this step, hydrogen atoms were added to the protein, cocrystallized ligand, and the hydroxide ion. Hydrogen atoms of the titratable residues were adjusted and side chains of Tyr, Thr, Ser, Asn, and Gln were optimized so that they could make better hydrogen bonding interactions. The structure was finally minimized such that the heavy atoms do not move beyond 0.3 Å from their starting positions. Structures of DHA and 7S-HDHA were modeled using the Edit/Build panel of Maestro and energy minimized using LigPrep software (Schrodinger Suite 2018-4, Schrodinger Inc.). Both DHA and 7S-HDHA were docked to the h15-LOX-1 model using the docking software Glide (version 8.1, Schrodinger Inc.) with the extra-precision docking score. We used the cocrystallized ligand coordinates to define the binding pocket. During the ligand-docking step, the protein was initially kept rigid, but despite extensive ligand conformation sampling, no low-energy docking pose was identified for the ligands. Therefore, we used InducedFit docking (Schrodinger Inc.), in which residues in the active site of the protein and ligand are treated flexibly. Specifically, during the initial docking step, side chains of Phe352, Ile413, Ile417, Met418, Cys559, and Leu588 were deleted to accommodate DHA and 7S-HDHA, because they appeared to block key portions of the active site. After generating the initial docking pose, side chain rotamers of these residues plus Arg402 and Gln595 (which have the potential to form hydrogen bonds with the ligand) were optimized. These docking and side chain optimization steps were iterated until a converged low energy docking pose was obtained.

For h15-LOX-2, structure-based docking calculations were performed using the available crystal structure of human ALOX15b (PDB entry 4nre). From the crystal structure, we retained the protein, Fe^{3+} ion, cocrystallized inhibitor, polyoxyethylene detergent (C8E), present in the active site, and a hydroxide ion that coordinates the metal ion; all other atoms were deleted. Prior to docking, the structure was subjected to the protein-preparation step using Maestro's Protein Preparation Wizard (Maestro version 11.8, Schrodinger Inc.). Although the cocrystallized inhibitor bound in a U-shaped binding mode, it did not have a carboxylate group, and it had only 21 atoms in the main chain as opposed to 22 atoms present in DHA or 7S-HDHA. Therefore, we performed flexible-receptor flexible-ligand docking using InducedFit docking software (Schrodinger Inc.). During InducedFit docking, only the following active site residues were treated flexibly: Phe365, Val426, Val427, Arg329, and Asp602.

RESULTS

Biosynthesis of 7S,14S-diHDHA

As discussed in the introduction, there are three proposed routes by which 7S,14S-diHDHA can be synthesized by LOXs (Scheme 1, pathways 1–3). These three pathways were therefore investigated in vitro to implicate possible in vivo biosynthetic routes. It should be emphasized that because these are di-oxygenation pathways, the di-hydroperoxide is formed in each of the pathways; however, the biologically isolated molecule, 7S,14S-diHDHA, is the reduced form due to cellular glutathione peroxidases.

Pathway 1: DHA with h12-LOX to 14S-HpDHA, then h5-LOX to 7S,14S-diHpDHA

The first possible route for biosynthesis of 7S,14S-diHDHA involves oxygenation of DHA by h12-LOX to form 14S-HpDHA (Scheme 1, pathway 1). In order to study the ability of h12-LOX to form 14S-HpDHA, steady state kinetics and product profiles were measured. The k_{cat} for h12-LOX with DHA was measured to be 14 s^{-1}, while the k_{cat}/K_M was found to be 13 $s^{-1}\mu M^{-1}$ (**Table 1**), demonstrating that

TABLE 1. Steady-state kinetic values of h12-LOX and h15-LOX-1 with DHA, 7S-HDHA, and 7S-HpDHA

Enzyme	Substrate	k_{cat} (sec^{-1})	k_{cat}/K_M ($sec^{-1}\mu M^{-1}$)	K_M (μM)
h12-LOX	AA	9.7 ± 1	5.8 ± 0.4	1.7 ± 0.3
	DHA	14 ± 1	13 ± 2	1.1 ± 0.2
	7S-HDHA	3.3 ± 0.2	1.8 ± 0.5	1.8 ± 0.5
	7S-HpDHA	0.68 ± 0.1	0.25 ± 0.1	2.7 ± 1
h15-LOX-1	AA	10 ± 1	2.1 ± 0.3	5.0 ± 0.3
	DHA	0.95 ± 0.1	0.68 ± 0.2	1.4 ± 0.3
	7S-HDHA	3.1 ± 0.1	0.51 ± 0.09	6.1 ± 0.5
	7S-HpDHA	0.57 ± 0.08	0.080 ± 0.02	6.9 ± 0.8

DHA is a comparable substrate to AA for h12-LOX in vitro (51, 52). The product profile indicates that the majority of oxylipin is oxygenated at C14 (greater than 80%), with minor amounts oxygenated at C11, as previously reported (53, 54).

After DHA reacts with h12-LOX to form 14S-HpDHA, it may subsequently react with h5-LOX to form 7(S),14(S)-dihydroperoxy-4Z,8E,10Z,12E,16Z,19Z-DHA (7S,14S-diHpDHA) (Scheme 1, pathway 1), the oxidized form of 7S,14S-diHDHA. In order to study the ability of h5-LOX to react with 14S-HDHA and 14S-HpDHA, steady-state kinetic values and product profiles were assessed, but no activity was observed by UV-VIS spectroscopy (i.e., no change in absorbance at 254, 270, or 302 nm being detected). Using the more sensitive LC-MS/MS method, the V_{max} values for 14S-HDHA and 14S-HpDHA were determined to be 0.00038 and 0.0015 ($mol/sec^{-1}/mol^{-1}$) at 10 μM substrate, respectively (**Table 2**). If we compare the V_{max} at 10 μM of DHA (vide supra), the V_{max} values of 14S-HDHA and 14S-HpDHA are 368-fold and 93-fold slower than that of DHA, indicating that 14-oxylipins are poor substrates of h5-LOX. Comparatively poor reactivity with oxygenated substrates has been demonstrated previously for soybean 15-LOX (55). Even with this lowered kinetic rate, the major product in both reactions was the 7S,14S-oxylipin, along with trace amounts of 8,14-oxylipin and tri-oxygenated products. Unfortunately, the low levels of tri-oxygenated products did not allow for reliable identification.

Pathway 2: DHA and h5-LOX to 7S-HpDHA, then h12-LOX to 7S,14S-diHpDHA (oxidized form of 7S,14S-diHDHA)

The second possible route for biosynthesis of 7S,14S-diHDHA begins with oxygenation of DHA by h5-LOX to form 7S-HpDHA (Scheme 1, pathways 2 and 3). The ability of h5-LOX to form products from DHA was assessed through kinetic measurements and product profiles. The V_{max} for DHA at 10 μM was determined to be 0.14 $mol/sec^{-1}/mol^{-1}$ (Table 2), similar to the reported value of 0.14 $mol/sec^{-1}/mol^{-1}$ for AA [converted from k_{cat} and K_M at 10 μM AA in (36)]. Interestingly, the reaction of h5-LOX with DHA was found to produce eight different products, with 7S-HpDHA being the major product at 52%, and seven minor products comprising the remaining 48% (**Table 3**, supplemental Fig. S1). The 4-product was not observed, consistent with results obtained from h5-LOX in neutrophils (37, 56) and monocytes (57). In macrophages, formation of 4-HDHA has been shown to occur independently of 5-LOX and 5-LOX-activating protein (FLAP) activity (58). It is important to note that the increased nonspecificity of h5-LOX with DHA relative to AA is a common observation for other LOX isozymes as well (see below). This appears to be a function of the structural difference between DHA and AA, with the increased length and unsaturation of DHA leading to a substrate-binding mode that promotes greater product diversity relative to AA.

The 7S-HpDHA produced by h5-LOX from DHA contains bis-allylic carbons that may react further with h12-LOX to produce the di-oxygenated oxylipin, 7S,14S-diHDHA

TABLE 2. V_{max} values of h5-LOX, h12-LOX, and h15-LOX-1 with DHA, 14S-HDHA, 14S-HpDHA, 7S-HDHA, and 7S-HpDHA

Enzyme	Substrate	V_{max} ($mol/sec^{-1}/mol^{-1}$)	7S,14S-diHDHA Biosynthetic Pathway Flux[a]
h5-LOX	DHA	0.14 ± 0.03	0.073
	14S-HDHA	0.00038 ± 0.0002	0.00038
	14S-HpDHA	0.0015 ± 0.0006	0.0015
h12-LOX	DHA	12 ± 1	9
	7S-HDHA	2.8 ± 0.2	2.3
	7S-HpDHA	0.53 ± 0.08	0.44
h15-LOX-1	DHA	0.84 ± 0.09	0.34
	7S-HDHA	1.9 ± 0.1	1.7
	7S-HpDHA	0.30 ± 0.4	0.19

Values determined at 10 μM substrate concentration. The V_{max} for h5-LOX was approximated by determining the amount of h5-LOX in the ammonium sulfate pellet by Western analysis relative to a known standard. Reactions with DHA represent the first step of the two biosynthetic steps, such as h15-LOX-1 V_{max} × percent 14S-HDHA, while reactions with oxylipins represent the second step of the two biosynthetic steps, such as h15-LOX-1 V_{max} × percent 7S,14S-HDHA.

[a]Biosynthetic flux is calculated by multiplying each V_{max} by the percentage of total product from that reaction that serves as substrate for the next step toward synthesis of 7S,14S-diHDHA.

TABLE 3. Distribution of products created by reaction of h5-LOX with DHA (10 μM)

Substrate	7-HpDHA	8-HpDHA	11-HpDHA	13-HpDHA	14-HpDHA	16-HpDHA	17-HpDHA	20-HpDHA
DHA	52 ± 9%	1 ± 1%	4 ± 2%	2 ± 1%	18 ± 4%	4 ± 2%	16 ± 6%	3 ± 2%

7S-HpDHA is the major product at 52% of the total, and seven minor products comprise the remaining 48%.

(Scheme 1, pathway 2). To test this possibility, steady-state kinetic values were determined for the reaction of h12-LOX with 7S-HDHA and 7S-HpDHA. The k_{cat}s for 7S-HDHA and 7S-HpDHA were found to be 3.3 s^{-1} and 0.68 s^{-1}, respectively, and the k_{cat}/K_Ms for 7S-HDHA and 7S-HpDHA were found to be 1.8 $s^{-1}\mu M^{-1}$ and 0.25 $s^{-1}\mu M^{-1}$, respectively (Table 1), which are markedly greater than the kinetic parameters of h5-LOX with the 14-oxylipins. The products of h12-LOX reacting with 7S-HDHA were exclusively di-oxygenated oxylipins, with 82% of 7S,14S-diHDHA and 18% of 7S,17S-diHDHA being generated (**Table 4**, supplemental Fig. S2). The production of 7S,17S-diHDHA is a remarkable result because h12-LOX is known to produce mostly 14S-HpDHA and only a minor amount of 11S-HpDHA from DHA (Table 4). The formation of 11S-HpDHA from DHA and h12-LOX indicates that DHA inserts deeper into the cavity for hydrogen atom abstraction at C9. However, with 7S-HDHA as the substrate, the minor product is 7S,17S-diHDHA, not 7S,11S-diHDHA, suggesting that 7S-HDHA does not enter as deeply into the active site, allowing for abstraction at C15 and the generation of 7S,17S-diHDHA. The reaction of 7S-HpDHA with h12-LOX produced comparable products as those from 7S-HDHA, indicating that no dehydration occurred to form the epoxide or its derivatives (Table 4).

Pathway 3: DHA and h5-LOX to 7S-HpDHA, then h15-LOX-1 to 7S,14S-diHpDHA (oxidized form of 7S,14S-diHDHA)

The third pathway involves the noncanonical reaction of h15-LOX-1 with 7S-HpDHA to produce 7S,14S-diHpDHA, which is subsequently reduced to 7S,14S-diHDHA (Scheme 1, pathway 3). h15-LOX-1 was reacted with DHA, 7S-HDHA, and 7S-HpDHA, demonstrating comparable rates between DHA and 7S-HDHA, but a slower rate for 7S-HpDHA, with k_{cat}/K_M values of 0.68, 0.51, and 0.08 $s^{-1}\mu M^{-1}$ for DHA, 7S-HDHA, and 7S-HpDHA, respectively (Table 1). Even more surprising, the k_{cat} value for 7S-HDHA was over 3-fold greater than that for DHA. These results indicate that DHA is still the more efficient substrate at low concentration (i.e., the fastest rate of substrate capture, k_{cat}/K_M) (59), but 7S-HDHA is an alternative substrate to DHA at high concentration, having the fastest rate of product release (k_{cat}) (59).

To determine the oxylipins generated by h15-LOX-1 from 7S-HDHA and 7S-HpDHA, the reaction products were isolated and analyzed via LC-MS/MS. Surprisingly, when h15-LOX-1 was reacted with 7S-HDHA, 90% of the products were 7S,14S-diHpDHA (i.e., the oxidized form of 7S,14S-diHDHA), with only 10% of 7(S),17(S)-dihydroperoxy-4Z,8E,10Z,13Z,15E,19Z-DHA (7S,17S-diHpDHA) being produced (**Table 5**, supplemental Fig. S3). Along with the primary di-HDHA products, minor amounts of tri-HDHA secondary products were produced in the reaction, representing less than 4% of the total and comprising mainly 7,16,17-triHDHA, indicating that the low ratio of 7S,17S-diHDHA to 7S,14S-diHDHA was not due to formation of tri-HDHA products. When 7S-HpDHA was used as the substrate, the products were comparable, with 65% 7S,14S-diHpDHA (i.e., the oxidized form of 7S,14S-diHDHA) and 35% 7S,17S-diHpDHA. The specificity of h15-LOX-1 and 7S-HDHA (90% 7,14-oxylipin) is markedly different than that seen with DHA where only 40% of the 14-oxylipin is observed. This difference is even more dramatic with AA as the substrate for h15-LOX-1, where only 10% of the ω-9 product, 12-HpETE, is made. To confirm the product structures, UV-VIS absorbance maxima, C18 reverse-phase retention times and MS/MS fragmentations were matched to known patterns for 7S,14S-diHDHA (supplemental Fig. S3), confirming that h15-LOX-1 has a different positional specificity in its reaction with 7S-HDHA than it does with DHA. For comparison, h15-LOX-1 reacts with DHA to generate 48% of the canonical ω-6 product, 17S-HpDHA, with a variety of minor products [40% 14S-HpDHA and 12% 11S-HpDHA (Table 5)] (18). The presence of 40% 14S-HpDHA is consistent with oxidation at the ω-9 position (10% 12-HpETE from AA); however, the observation of the 11S-HpDHA minor product is unusual and indicates that the added length and unsaturation of DHA leads to multiple productive catalytic poses of DHA in h15-LOX-1, similar to those

TABLE 4. Distribution of products produced by h12-LOX with 7S-HDHA (10 μM), as determined by LC-MS/MS

Substrate	14-Product	17-Product
7S-HDHA	82 ± 6%	18 ± 4%
7S-HpDHA	79[a] ± 4%	18 ± 3%

The major product of the reaction of h12-LOX with 7S-HDHA is 7S,14S-diHpDHA. Note that the abbreviations "14-Product, etc." in the column headings are used to simplify the complexity of the table labels.

[a] A peak of approximately 3% of the total area was observed that had a parent mass of a di-HDHA; however, its exact nature was undetermined due to its small area.

TABLE 5. Distribution of products generated by h15-LOX-1 with DHA, 7S-HDHA, and 7S-HpDHA (10 μM), as determined by LC-MS/MS

Substrate	11-Product	14-Product	17-Product
DHA[a]	12 ± 1%	40 ± 5%	48 ± 4%
7S-HDHA	0	90 ± 6%	10 ± 6%
7S-HpDHA	0	65 ± 8%	35 ± 8%

h15-LOX-1 shows altered positional specificity when reacting with 7S-HDHA and 7S-HpDHA. Note that the abbreviations "11-Product, etc." in the column headings are used to simplify the complexity of the table labels.

[a] These data were previously published (18)

seen with h5-LOX. These rates and product profiles support both pathways 2 and 3 (Scheme 1) as the most likely in vitro biosynthetic routes for 7S,14S-diHDHA production.

Reaction of 7S-HDHA and 7S-HpDHA with h15-LOX-2 in biosynthesis of 7S,17S-diHDHA

As observed above, h15-LOX-1 only produces a small amount of 7S,17S-diHDHA when reacting with 7S-HDHA. This result raises the possibility that h15-LOX-2 could be the primary LOX isozyme responsible for the generation of 7S,17S-diHDHA (RvD5). In order to study this reaction further, h15-LOX-2 was reacted with DHA, 7S-HDHA, and 7S-HpDHA, and all three were determined to have comparable rates (**Table 6**). The k_{cat} for DHA was 3.0 s^{-1}, the k_{cat} for 7S-HDHA was 2-fold higher at 5.8 s^{-1}, while the k_{cat} for 7S-HpDHA was 3.4 s^{-1}. Due to the lower K_M for DHA, the k_{cat}/K_M for DHA was 2-fold greater than that of 7S-HDHA (k_{cat}/K_M = 0.15 $s^{-1}\mu M^{-1}$) and 3-fold greater than 7S-HpDHA (k_{cat}/K_M = 0.08 $s^{-1}\mu M^{-1}$). These values indicate that DHA has the fastest rate of substrate capture at low substrate concentrations, k_{cat}/K_M, but 7S-HDHA has the fastest rate of product release at high substrate concentrations, k_{cat} (59). For comparison, the kinetic parameters for h15-LOX-2 and AA are 0.96 s^{-1} for k_{cat} and 0.19 $s^{-1}\mu M^{-1}$ for k_{cat}/K_M, similar to published values (15, 51), indicating that at low substrate concentration, 7S-HDHA is a comparable substrate to that of AA, but DHA is preferred. These data support pathway 5 (Scheme 1) as the most likely in vitro biosynthetic route for RvD5 production.

To determine the oxylipins produced by h15-LOX-2 from DHA, 7S-HDHA, and 7S-HpDHA, the reaction products were isolated and analyzed via LC-MS/MS. The reaction of h15-LOX-2 with DHA produced 95% 17S-HDHA, 3% 14S-HDHA, and 2% 20-HDHA (supplemental Fig. S4), similar to its high level of specificity with AA as the substrate (i.e., greater than 95% 15-HpETE) and consistent with the literature (36). The reaction of 7S-HDHA with h15-LOX-2 produced 100% 7S,17S-diHDHA (supplemental Fig. S5), while reaction with 7S-HpDHA produced 98% 7S,17S-diHDHA and 2% 7S,20-HDHA (**Table 7**). The 7S,17S-diHDHA produced by h15-LOX-2 from 7S-HDHA was compared with standards and found to have identical UV-VIS maxima, LC-MS/MS retention time, and fragmentation as 7S,17S-diHDHA (RvD5). It should be noted that no products were observed from the reaction of h15-LOX-2 with either 17S-HDHA or 17S-HpDHA using UV-VIS spectroscopy or LC-MS/MS, indicating that 7S,17S-diHDHA is not biosynthesized through the reverse orientation of the substrate. In addition, h15-LOX-2 was not observed to produce the 16,17-epoxide product from 17S-HpDHA, reinforcing its selective reactivity to abstracting only from the ω-8 carbon to produce the ω-6 oxygenation product.

TABLE 6. Steady-state kinetic values for h15-LOX-2 with DHA, 7S-HDHA, and 7S-HpDHA

Substrate	k_{cat} (sec^{-1})	k_{cat}/K_M ($sec^{-1}\mu M^{-1}$)	K_M (μM)
AA	0.96 ± 0.09	0.19 ± 0.02	5.0 ± 0.3
DHA	3.0 ± 0.3	0.27 ± 0.03	11 ± 2
7S-HDHA	5.8 ± 0.4	0.15 ± 0.02	40 ± 4
7S-HpDHA	3.4 ± 0.4	0.08 ± 0.01	41 ± 7

TABLE 7. Distribution of products made from h15-LOX-2 with DHA, 7S-HDHA, 7S-HpDHA, 17S-HDHA, and 17S-HpDHA (10 μM), as determined by LC-MS/MS

Substrate	14-Product	17-Product	20-Product
DHA	3 ± 1%	95 ± 2%	2 ± 1%
7S-HDHA	0%	100 ± 1%	0%
7S-HpDHA	0%	98 ± 1%	2 ± 1%
17S-HDHA	No reaction	No reaction	No reaction
17S-HpDHA	No reaction	No reaction	No reaction

No reaction was detectable after the incubation of h15-LOX-2 with either 17S-HDHA or 17S-HpDHA. Note that the abbreviations "14-Product, etc." in the column headings are used to simplify the complexity of the table labels.

Formation of 7S,17S-diHDHA by h5-LOX from 17S-HDHA and 17S-HpDHA

17S-HDHA was reacted with h5-LOX to investigate the rate of 7S,17S-diHDHA synthesis, relative to the production of 7S,17S-diHDHA from h15-LOX-2 and 7S-HDHA. Despite achieving complete turnover of DHA with h5-LOX in ∼1 min, an identical amount of h5-LOX did not produce an observable reaction with 17S-HDHA or 17S-HpDHA when monitoring at 254 and 270 nm, using UV-VIS spectroscopy. However, analyzing the reaction at multiple time points using LC-MS/MS allowed for the estimation of the V_{max} value. Compared with the reaction of h5-LOX with AA and DHA, the reaction rates with 17S-HDHA and 17S-HpDHA were over 100-fold slower (**Table 8**). The products of the reaction of h5-LOX with both 17S-HDHA and 17S-HpDHA were approximately 90% 7S,17S-diHDHA, along with minor amounts of 16,17-diHDHA and 10,17-diHDHA. For comparison, similar reactions were performed with h15-LOX-2 and the 7S-oxylipins, and the V_{max} rates were significantly greater than observed with h5-LOX (Table 8), indicating that pathway 6 in Scheme 1 is not efficient in vitro. As with h15-LOX-2, it is possible that 7S,17S-diHDHA could also be biosynthesized through a reverse binding orientation to h5-LOX, however, no reaction was observable between h5-LOX and 7S-HDHA or 7S-HpDHA, using UV-VIS spectroscopy. When analyzed by LC-MS/MS, 7S,17S-diHDHA was observed, but the reaction rates of h5-LOX with 7S-HDHA and 7S-HpDHA were over 1,000-fold slower than with AA and DHA and were considered inconsequential (i.e., no reaction).

Chiral chromatography characterization of 7S,14S-diHDHA and 7S,17S-diHDHA (RvD5)

We predicted that the oxygen on C14 of 7S,14S-diHDHA is in the S-configuration because h15-LOX-1 typically performs stereospecific oxygenation generating the S-configured product when the substrate enters the active site methyl-end first. To determine the relative stereochemistry of the 7S,14S-diHDHA produced by reacting 7S-HDHA with h15-LOX-1, the products of this reaction were isolated, reduced, and compared with standards via reverse phase chiral chromatography. MaR1 and 7-epi-MaR1 standards (Cayman Chemicals) and the 7S,14S-diHDHA produced by

TABLE 8. V_{max} values of reaction steps in the biosynthesis of RvD5 were calculated at 10 μM substrate concentration for comparison

Enzyme	Substrate	V_{max} (mol/sec^{-1}/mol^{-1})	7S,17S-diHDHA Biosynthetic Pathway Flux[a]
h5-LOX	DHA	0.14 ± 0.03	0.073
	17S-HDHA	0.0012 ± 0.0004	0.0012
	17S-HpDHA	0.0014 ± 0.0005	0.0014
h12-LOX	DHA	12 ± 1	0
	7S-HDHA	2.8 ± 0.2	0.5
	7S-HpDHA	0.53 ± 0.08	0.1
h15-LOX-2	DHA	1.3 ± 0.1	1.3
	7S-HDHA	1.2 ± 0.1	1.2
	7S-HpDHA	0.67 ± 0.08	0.65
h15-LOX-1	DHA	0.84 ± 0.09	0.39
	7S-HDHA	1.9 ± 0.1	0.19
	7S-HpDHA	0.30 ± 0.04	0.11

Reactions with DHA represent the first step of the two biosynthetic steps, such as h15-LOX-1 V_{max} × percent 17S-HDHA, while reactions with oxylipins represent the second step of the two biosynthetic steps, such as h15-LOX-1 V_{max} × percent 7S,17S-HDHA.

[a]Biosynthetic flux is calculated by multiplying each $V_{max.}$ by the percentage of total product from that reaction that serves as substrate for the next step in the synthesis of 7S,17S-diHDHA.

h15-LOX-1 from 7S-HDHA eluted at distinct times when analyzed via chiral HPLC (**Fig. 2**). 7-epi-MaR1 eluted with a retention time of 45.5 min, MaR1 with a retention time of 37.9 min, and the enzymatically-synthesized 7S,14S-diHDHA eluted with a retention time of 22.4 min. All three compounds shared identical fragmentations when analyzed via LC/MS/MS. As no 7R,14S-EZE-diHDHA or 7S,14S-EZE-diHDHA standards are commercially available, resolution of these two isomers from one another was confirmed by reacting h15-LOX-1 with a racemic mixture of 7R/S-HDHA, resulting in two peaks at 20.8 and 22.4 min with identical fragmentations and UV-spectra. Because h5-LOX also typically generates product in the S-configuration from substrates that enter the active site methyl-end first, the reaction of h5-LOX with 14S-HDHA is predicted to produce 7S,14S-diHDHA. A comparison of this product with that generated by h15-LOX-1 from 7S-HDHA revealed a chiral retention time of 22.4 min, identical to that of the 7,14-diHDHA

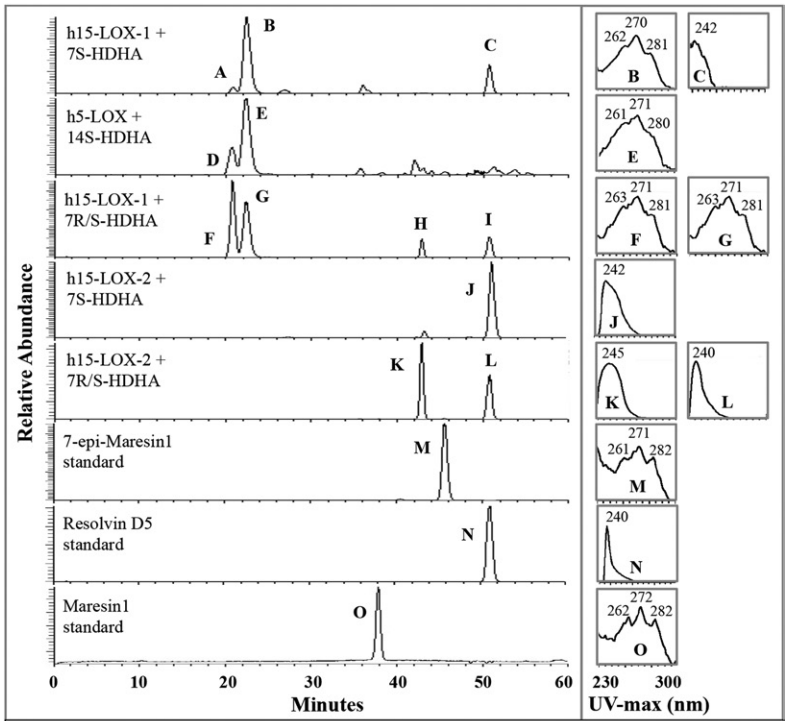

Compound	Stereochemistry	Peaks	Retention Time
7R,14S-diHDHA	7(R),14(S)-dihydroxy-4Z,8E,10Z,12E,16Z,19Z-DHA	A,D,F	20.8 min
7S,14S-diHDHA	7(S),14(S)-dihydroxy-4Z,8E,10Z,12E,16Z,19Z-DHA	B,E,G	22.4 min
MaR1	7(R),14(S)-dihydroxy-4Z,8E,10E,12Z,16Z,19Z-DHA	O	37.9 min
7R,17S-diHDHA	7(R),17(S)-dihydroxy 4Z,8E,10Z,13Z,15E,19Z-DHA	H,K	43.2 min
7-epi-MaR1	7(S),14(S)-dihydroxy-4Z,8E,10E,12Z,16Z,19Z-DHA	M	45.5 min
7S,17S-diHDHA	7(S),17(S)-dihydroxy 4Z,8E,10Z,13Z,15E,19Z-DHA	C,I,J,L,N	51.0 min

Fig. 2. Chiral chromatograms and UV-maxima of 7,14-diHDHA and 7,17-diHDHA isomers. The products formed by h15-LOX-1 and h15-LOX-2 from 7S-HDHA and 7R/S-HDHA and by h5-LOX from 14S-HDHA were analyzed via chiral LC-MS/MS and UV spectra and compared with MaR1, 7-epi-MaR1, and RvD5 standards. All 7,14-diHDHA isomers contained a central peak at ~270 nm, surrounded by shoulders at ~260 and ~280 nm, consistent with the presence of a conjugated triene. Shoulders of equal intensity at 281 and 261 nm are indicative of an EEZ configuration, while a more intense shoulder at 260 nm compared with 280 nm indicates the EZE configuration. 7,17-diHDHA isomers contain two conjugated dienes, with UV-maxima of 240–245 nm, distinguishing them from 7,14-diHDHA.

produced by h15-LOX-1 from 7S-HDHA. This indicates that both oxylipins are 7S,14S-diHDHA, just produced through a different order of LOX biosynthetic steps. While it is conceivable that both h15-LOX-1 and h5-LOX change their product profile and generate the R-configuration oxylipin, this is not the case based on the chiral column results. It should be noted that a small 7R,14S peak is generated by the reaction of 14S-HDHA with h5-LOX. In addition, a small 7R,14S-diHDHA peak is generated by the reaction of 7S-HDHA with h15-LOX-1, indicating that the 7S-HDHA synthesized by h5-LOX from DHA contained a small contaminate of 7R-HDHA. Together, these two observations indicate that while the major product of h5-LOX is the S-configured product, a small amount of the R-product is also made.

Along with chiral retention times, UV spectra were compared to further differentiate the double bond geometry of the various products. All 7,14-diHDHA products contained a central peak at ∼270 nm, surrounded by shoulders at ∼260 nm and ∼280 nm, consistent with the presence of a conjugated triene. In Mar1 and 7-epi-MaR1, the shoulders at 281 and 261 nm were of equal intensity, indicative of a conjugated triene with EEZ configuration (60–62). In contrast, the 7,14-HDHA produced enzymatically showed a more intense shoulder at 260 nm than at 280 nm, indicating the EZE configuration (63). It should be noted that we have attempted to determine the absolute stereochemistry of 7S,14S-diHpDHA by generating the double Mosher derivative, but unfortunately low yields from enzymatic synthesis and NMR peak overlap prohibits the assignment of the molecules' stereochemistry.

To determine the relative stereochemistry of the 7,17-oxylipin produced by h15-LOX-2 and 7S-HDHA, the molecule was compared with an RvD5 standard using reverse-phase chiral HPLC coupled to MS/MS. The chiral HPLC retention time, MS/MS fragmentation, and UV-spectra of the 7,17-oxylipin produced by h15-LOX-2 from 7S-HDHA matched those of the RvD5 standard (Cayman Chemicals) (Fig. 2), strongly suggesting its identity to be 7S,17S-diHDHA (RvD5). 7S,17S-diHDHA and 7R,17S-diHDHA were resolved under these conditions and demonstrated UV-maxima of 240–245 nm, indicative of two separate conjugated dienes

Molecular modeling of DHA and 7S-HDHA bound to h15-LOX-1

The shift in product profile seen between h15-LOX-1 reacting with DHA and 7S-HDHA suggests that these substrates must bind differently in the active site, and therefore molecular modeling was employed to assess this possibility. Extra-precision Glide scores were used to approximate ligand binding free energy, with lower negative scores representing tighter binding (64). **Figure 3** shows the InducedFit docking poses of DHA and 7S-HDHA with h15-LOX-1, with corresponding extra-precision docking scores for these poses of −9.5 and −10.8, respectively. In the docking model, the carboxylate groups of both DHA and 7S-HDHA form hydrogen bonds with the side chain of Arg402 and the hydrophobic tails of both substrates are buried deep in the hydrophobic pocket created by residues Phe352, Ile417, and Ile592. This aligns with previous structural work carried out on h15-LOX-1 (65). However, a key difference is that the C7 hydroxyl group of 7S-HDHA forms a hydrogen bond with the backbone carbonyl oxygen of Ile399. This difference in binding between DHA and 7S-HDHA is manifested in their distances between the iron-hydroxide oxygen atom and the hydrogen on the reactive carbons, C12 and C15. The modeling data indicate that for 7S-HDHA, the C12 pro-S hydrogen is markedly closer (2.6 Å) to the iron-hydroxide moiety than C15 hydrogen (5.9 Å) (**Table 9**). Considering that C12 hydrogen atom abstraction leads to 7S,14S-diHDHA, while C15 hydrogen atom abstraction leads to 7S,17S-diHDHA, these docking results are consistent with the enzymatic results. For DHA, the distance for the C15 pro-S hydrogen (3.8 Å) is slightly shorter than that of C12 (4.1 Å), consistent with the experimental results, but the distance difference is not as distinct as that for 7S-HDHA, possibly due to the more homogeneous hydrophobic nature of DHA compared with 7S-HDHA.

Molecular modeling of DHA and 7S-HDHA bound to h15-LOX-2

For h15-LOX-2, we used the same InducedFit docking method with the extra-precision scoring function. The extra-precision docking score of the low-energy docking pose of DHA and 7S-HDHA against h15-LOX-2 are −7.09 and −9.31, respectively, and their docking poses are shown in

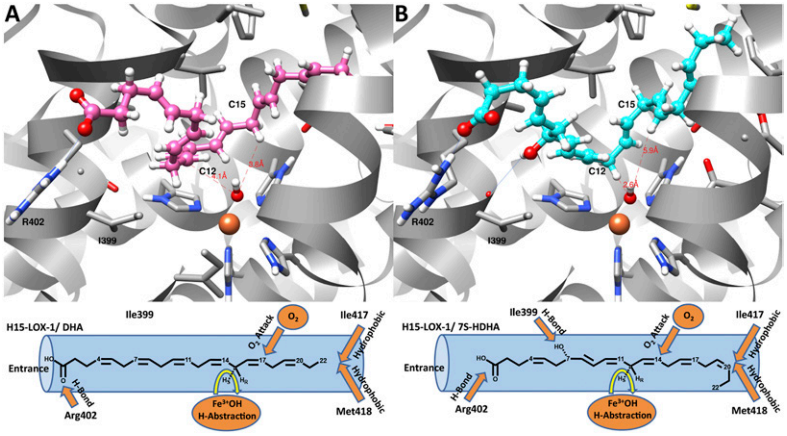

Fig. 3. InducedFit docking poses of DHA (A) and 7S-HDHA (B) against the active site of h15-LOX1. DHA and 7S-HDHA atoms, hydroxide ion, and metal ion are shown in ball-and-stick representation. Protein residues are shown in stick representations. Carbon atoms of DHA, 7S-HDHA, and protein are shown in pink, cyan, and gray, respectively; nitrogen, oxygen, and hydrogen atoms are shown respectively in blue, red, and white. Fe^{3+} is shown in orange. Hydroxide oxygen to C12-hydrogen and C15-hydrogen distances of DHA and 7S-HDHA are also shown. Below each docking structure, a cartoon representation is presented for positional emphasis.

TABLE 9. Distances between the hydroxide ion and oxygen atom and the pro-S hydrogens of the reactive carbons (C12 and C15) of DHA and 7S-HDHA against h15-LOX-1

Substrate	Hydroxide Oxygen to pro-S C12-Hydrogen Distance (Å)	Hydroxide Oxygen to pro-S C15-Hydrogen Distance (Å)
DHA	4.1	3.8
7S-HDHA	2.6	5.9

TABLE 10. Distances between the hydroxide ion and oxygen atom and the pro-S hydrogen of the reactive carbons (C12 and C15) of DHA and 7S-HDHA with h15-LOX-2

Substrate	Hydroxide Oxygen to pro-S C12-Hydrogen Distance (Å)	Hydroxide Oxygen to pro-S C15-Hydrogen Distance (Å)
DHA	7.2	4.1
7S-HDHA	4.0	2.7

Fig. 4. Both substrates bind into the active site tail first, utilizing a U-shaped binding mode. The carboxylate groups of both DHA and 7S-HDHA make a salt-bridge interaction with the R429 residue on the helix α12. In contrast, h15-LOX-1 utilizes R402 (helix α11) to hydrogen bond with the carboxylate group of the substrate, previously reported to be important for catalysis (65), possibly leading to their different product specificities. The hydrophobic tails of both substrates are buried deeply in the hydrophobic pocket created by residues F365, L420, I421, V427, F438, and L607. The hydroxyl group of 7S-HDHA makes a hydrogen-bond to the backbone carbonyl oxygen of L419. The distance between reactive pro-S hydrogen of C15 and the oxygen atom of the hydroxide ion is 4.1 Å and 2.7 Å for DHA and 7S-HDHA, respectively (**Table 10**). These distances are shorter than the pro-S hydrogen of C12 and the oxygen atom of the hydroxide ion for DHA and 7S-HDHA (7.2 Å and 4.0 Å, respectively) (Table 10). These two binding modes are consistent with the enzymatic reaction involving abstraction of the pro-S hydrogen from C15 for both DHA and 7S-HDHA, to produce the 17-product exclusively (Table 10) (66–70) and not the 14-product from C12 hydrogen abstraction.

Effect of 7S,14S-diHDHA and RvD5 on platelets

Previous studies have shown that DHA and the h12-LOX-derived oxylipins of DHA have antiplatelet effects (71). Therefore, to determine the effect of RvD5, 7S,14S-diHDHA, and related maresin isomers on platelet activation, washed platelets were treated with oxylipins in half-log increments and then stimulated with collagen (0.25 μg/ml) in an aggregometer. 7S,14S-diHDHA fully inhibited platelet aggregation at 10 μM, while reducing aggregation by 65% at 3 μM. (**Fig. 5**). Platelets treated with 3 and 10 μM of RvD5 had an approximate reduction in aggregation of 65% and 90%, respectively, while MaR1 and 7-epi-MaR1 were the least potent, reducing aggregation by approximately 70% at 10 μM. 12(S)-8Z,10E,14Z-hydroxy-eicosatrienoic acid (12S-HETrE), a h12-LOX-derived oxylipin of dihomo-gamma-linoleic acid (DGLA) with known antiplatelet activity (72–74), displayed slightly greater potency than 7S,14S-diHDHA and 7S,17S-diHDHA (RvD5), reducing collagen-mediated platelet aggregation by 68% at 1 μM. Together, this data demonstrates that 12-HETrE was more potent than both 7S,17S-diHDHA (RvD5) and 7S,14S-diHDHA for inhibiting collagen-induced platelet aggregation; however, at 10 μM, all three molecules inhibited aggregation completely. It should be noted that these conditions (0.25 μg/ml collagen as activator) are more sensitive to inhibition than our previously published conditions (20 μM PAR1-AP as agonist) (73) and therefore demonstrate a greater effect on aggregation at lower concentrations of 12S-HETrE.

Platelet lipidomics with 7S-HDHA

The reduction in aggregation seen in platelets incubated with 7S-HDHA could be caused by either the 7S-HDHA itself or by a biosynthetic product produced by platelets during incubation. To investigate the latter possibility, platelets were incubated with 7S-HDHA and analyzed for the presence of 7S-HDHA metabolites using LC-MS/MS. Although large amounts of unreacted 7S-HDHA were detectable in the samples, no levels of any di-HDHAs or tri-HDHAs were detectable. As a control, platelets incubated with 5S-HETE were also analyzed for the presence of 5S-HETE metabolites. Although large levels of 12-HETE were detectable from endogenous AA, no appreciable levels of 5S-HETE/h12-LOX metabolites were detectable down to 2 ng/ml. This is an unexpected result because h12-LOX is capable of reacting with 7S-HDHA in vitro to produce

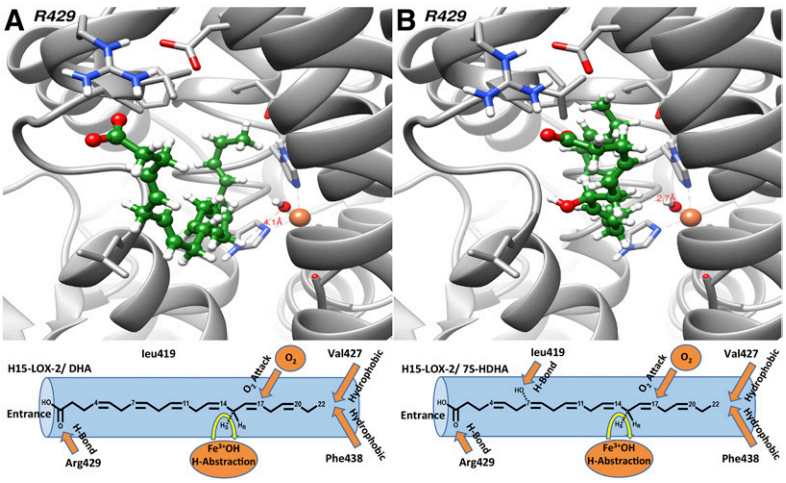

Fig. 4. InducedFit docking poses of DHA (A) and 7S-HDHA (B) against the h15-LOX-2 active site. DHA and 7S-HDHA atoms, hydroxide ion, and metal ion are shown in ball-and-stick representation and protein residues are shown in stick representation. Carbon atoms of DHA and 7S-HDHA are shown in green color and proteins are shown in gray color; nitrogen, oxygen, and hydrogen atoms are shown respectively in blue, red and, white colors. Fe^{3+} ion is shown in orange. The distance between the reactive pro-S hydrogen atom of C15 and the oxygen atom of the hydroxide ion is 4.1 Å and 2.7 Å for DHA and 7S-HDHA, respectively (values not shown). Below each docking structure, a cartoon representation is presented for positional emphasis.

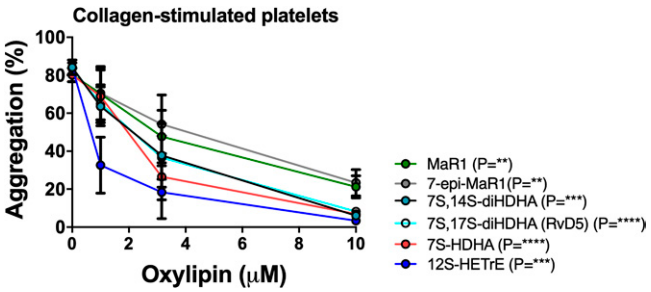

Fig. 5. The effect of MaR1, 7-epi-MaR1, 7S,14S-diHDHA, 7S,17S-diHDHA (RvD5), 7S-HDHA, 12SHETrE, Mar1, and 7-epi-Mar1 on aggregation of activated platelets. Washed human platelets were treated with vehicle (DMSO) or MaR1, 7-epi-MaR1, 7S,14S-diHDHA, 7S,17S-diHDHA, 7S-diHDHA, or 12S-HETrE in half-log increments ranging from 1 to 10 μM for 10 min and then stimulated with collagen (0.25 μg/ml) in an aggregometer. Note that the data for 7S,14S-diHDHA and 7S,17S-diHDHA are nearly identical and thus overlap significantly. Data represent the mean ± SEM of five independent experiments. Statistical analysis was performed using the one-way ANOVA test comparing the aggregation of platelets treated with each concentration of oxylipin to the aggregation of vehicle-treated platelets. $^{**}P < 0.01$, $^{***}P < 0.001$, $^{****}P < 0.0001$.

7S,14S-diHDHA. The fact that no 7S,14S-diHDHA is produced suggests that 7S-HDHA is most likely the bioactive species; however, we cannot discount the possibility that a trace product that has significantly higher biological activity is the active species. In addition, it is surprising that 7S-HDHA does not react appreciably with h12-LOX in the cellular milieu of the platelet, considering the ability of h12-LOX to react with 7S-HDHA in vitro. We are currently investigating this result in more detail with the hypothesis that a component of the cellular milieu, such as a protein, or small molecule affects h12-LOX reactivity.

DISCUSSION

Biosynthesis of 7S,14S-diHDHA

7S,14S-diHDHA is an analog of MaR1 (17) and is proposed to have a distinct biosynthetic pathway from MaR1. Its structure suggests three possible routes for its biosynthesis. Pathway 1 involves the oxidation of DHA at C14 by h12-LOX, followed by oxidation at C7 by h5-LOX; however, the in vitro data of this work suggests this is a very unfavorable biosynthetic route. Although DHA is a good substrate for h12-LOX, forming 14S-HpDHA at a rate similar to 12S-HpETE formation from AA (52), the second step in this pathway is kinetically unfavorable (Table 2).

For pathway 2 in Scheme 1, DHA is oxidized at C7 by h5-LOX followed by oxidation at C14 by h12-LOX. In comparison to pathway 1, pathway 2 is a kinetically favorable in vitro biosynthetic route. The first step, formation of 7S-HpDHA from DHA by h5-LOX, occurs rapidly with a V_{max} comparable to that of AA kinetics. The second step is also favorable, as the reaction of h12-LOX with 7S-HDHA has k_{cat} and k_{cat}/K_M values that are within 10-fold the rate of DHA. The slowest step in this pathway (i.e., the rate-determining step) is over 350 times faster than the reaction of h5-LOX with 14S-HDHA.

Interestingly, pathway 2 also presents a possible novel pathway to biosynthesizing 7S,17S-diHDHA (RvD5) with h12-LOX. The production of 7S,17S-diHpDHA is 18% of that of 7S,14S-diHpDHA, which is a significant percentage given the potency of RvD5 (25). The result also indicates a product promiscuity rarely seen for h12-LOX. h12-LOX produces over 95% 12S-HpETE from AA, so to produce 18% 7S,17S-diHpDHA is noteworthy. Another interesting aspect of this result is the mechanism of 7S,17S-diHpDHA formation. For 7S,17S-diHpDHA to form, h12-LOX must abstract from C15 of 7S-HpDHA, which indicates that the methyl tail of 7S-HpDHA is not positioned as deep in the active site pocket as that for 7S,14S-diHpDHA formation. These data suggest that the alcohol on C7 of 7S-HpDHA could interact with the active site and prevent the full penetration of the methyl tail into the bottom of the active site pocket.

The final biosynthetic route examined, pathway 3, is the oxidation of DHA at C7 by h5-LOX followed by oxidation at C14 by h15-LOX-1 and is a noncanonical pathway. h15-LOX-1 reacts with DHA and produces a majority of 17S-HpDHA (48%), with a smaller amount of 14S-HpDHA (40%). As shown with AA (65), product specificity is dictated by the methyl end of the fatty acid, with the majority of oxygenation occurring on the ω-6 carbon (C15 for AA and C17 for DHA), with a minority occurring on the ω-9 carbon (C12 for AA and C14 for DHA). Therefore, it is reasonable to expect a similar distribution of products with 7S-HDHA as the substrate; however, this is not the case. Pathway 3 produces over 9-fold more of 7S,14S-diHDHA than 7S,17S-diHDHA. In addition, this unusual product pathway is kinetically favorable in vitro. Both the first step, formation of 7S-HpDHA from DHA by h5-LOX, and the second, reaction of 7S-HDHA with h15-LOX-1, occur relatively rapidly. These results indicate that, although the hydroxyl group on C7 has a large effect on the positional specificity of the enzyme, it has little effect on catalysis, leading to a favorable overall kinetic condition. In summary, if we consider the product of both the rate and the percent product formation (i.e., the biosynthetic flux, **Scheme 2**), the data indicate that the most efficient pathway for making 7S,14S-diHDHA is thru h5-LOX and then h12-LOX or h15-LOX-1 and not vice versa because the reaction of h5-LOX with 14-HpDHA is markedly slower and hence rate-limiting.

Although changes in the positional specificity of LOXs have been demonstrated before (20), the finding that h15-LOX-1 primarily oxygenates C17 on DHA, but C14 on 7S-HDHA, is surprising. In order to obtain a better understanding of this binding event, DHA and 7S-HDHA were docked to a model of h15-LOX-1. In the case of DHA, both C12 and C15 are at a reasonable distance for hydrogen abstraction (75), whereas in case of 7S-HDHA, C12 is closer to the metal ion than C15, supporting the experimental results (Table 9). The model explains this result by having the hydroxyl group at C7 in 7S-HDHA forming a hydrogen bond with the backbone carbonyl of I399, which subsequently positions C12 closer to the metal ion. Without a similar restraint, the flexibility of DHA positions both C12 and C15 close to the metal

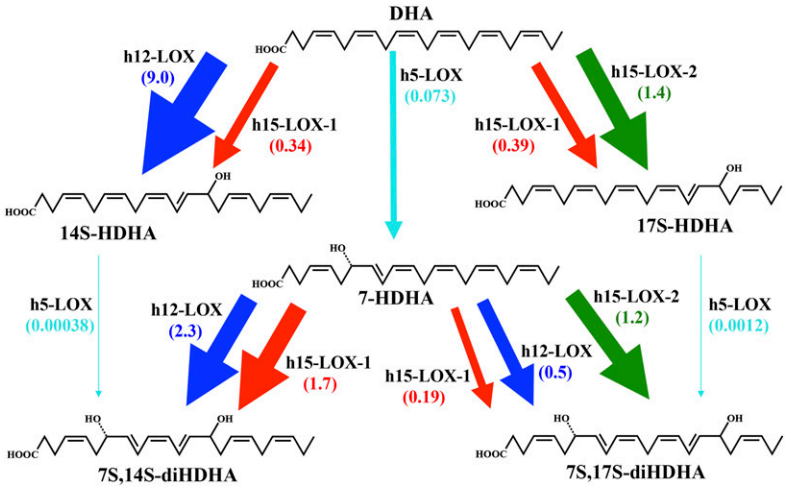

Scheme 2. Comparison of pathways for the biosynthesis of RvD5 and 7S,14S-diHDHA. The total biosynthetic flux for the reactions of h5-LOX, h12-LOX, and h15-LOX-1 with DHA, 14S-HpDHA, and 7SHpDHA are compared by multiplying V_{max} values (mol/sec^{-1}/mol^{-1}) at 10 μM substrate by the percent product for each reaction. In all pathways, turnover by h5-LOX is the rate-limiting step, and we have assumed that the hydroperoxides are reduced to the alcohols.

ion, helping to explain the greater number of products made by h15-LOX-1 from DHA compared with AA. This model suggests that 7S-HDHA is positioned further inside the active site than DHA, overcoming steric interactions to position C12 for hydrogen atom abstraction (Fig. 3). We are currently investigating the active site of h15-LOX-1 with mutagenesis to better understand the binding requirements of h15-LOX-1 in more detail.

Biosynthesis of 7S,17S-diHDHA (RvD5)

The discovery of pathway 3 as a relevant route to the biosynthesis of 7S,14S-diHDHA raises questions with respect to the biosynthetic route to making 7S,17S-diDHA (RvD5). Previously, 7S,17S-diDHA (RvD5) was proposed to be biosynthesized from DHA in two steps: initial oxygenation of C7 by h5-LOX followed by oxygenation of C17 by h15-LOX-1 (27, 28). This hypothesis was based on the prevalence of h15-LOX-1 in the inflammasome and the preference of h15-LOX-1 to oxygenate DHA at C17. However, our work shows that h15-LOX-1 shifts its positional specificity when reacting with 7S-HDHA in vitro, mainly creating 7S,14S-diHDHA and very little 7S,17S-diHDHA. This marked change in substrate specificity indicates that another LOX, such as h15-LOX-2, could be responsible for the biosynthesis of RvD5.

h15-LOX-2 reacts favorably with DHA, compared with AA, EPA, DGLA, and GLA (76), indicating that h15-LOX-2 maintains similar rates of product release (k_{cat}) across a wide range of fatty acid substrates (59). Because the reaction of h15-LOX-2 with DHA produces 95% 17S-HDHA, and the fact that h15-LOX-1-specific inhibitors do not block production of 17S-HDHA in neutrophils and eosinophils (44), it is possible that h15-LOX-2 is the source of 7S,17S-diHDHA because 7S-HDHA and 7S-HpDHA are viable substrates of h15-LOX-2, with greater k_{cat} values than DHA.

With respect to the biosynthetic pathway of RvD5, the fact that RvD5 contains two hydroxyls on C7 and C17 suggests three likely routes for the biosynthesis of RvD5 from DHA (pathways 4, 5, and 6, Scheme 1). The first route could be the oxygenation at C7 by h5-LOX followed by oxygenation of C17 by a 15-LOX isozyme (Pathway 4 or 5), either h15LOX-1 or h15-LOX-2. The second route is the reverse, with oxygenation of C17 by a 15-LOX isozyme, followed by oxygenation of C7 by h5-LOX (pathway 6). In the current study, we find that h5-LOX reacts well with DHA; however, it reacts significantly more slowly with 7S-HDHA and 17S-HDHA. For a direct comparison, the V_{max} at 10 μM substrate was determined to be 0.14 mol/sec^{-1}/mol^{-1} for h5-LOX with DHA (Table 8), which is over 100 times greater than the rate observed with 17S-HDHA (V_{max} = 0.0012 mol/sec^{-1}/mol^{-1} at 10 μM). This is consistent with the low reactivity of h5-LOX and 14S-HDHA, indicating that h5-LOX does not react well with oxygenated derivatives of DHA and brings into question pathway 6 as a viable in vivo biosynthetic route. Pathway 4 also appears unfavorable because the current work indicates that h15-LOX-1 reacts with 7S-HDHA to produce 90% 7S,14S-diHDHA (see above). It therefore appears that h15-LOX-1 may not contribute significantly to the in vitro biosynthesis of RvD5. h15-LOX-2, however, reacts well with 7S-HDHA (V_{max} = 1.2 mol/sec^{-1}/mol^{-1} at 10 μM) (Table 8), indicating that the rate of oxygenation at C7 by h5-LOX followed by oxygenation of C17 by h15-LOX-2 is a markedly faster pathway than the rate of oxygenation of C17 by h15-LOX-2 followed by oxygenation of C7 by h5-LOX. Therefore, if we calculate the biosynthetic flux [i.e., the rates multiplied by the percent product formation (Scheme 2)], it is apparent that the preferred pathway of RvD5 production in vitro is thru h5-LOX and then h15-LOX-2.

The h15-LOX-2 active site tolerates substrates which are oxygenated close to the carboxylate end (15), which is consistent with the methyl-end of the substrate binding at the bottom of the active site (65, 77, 78), allowing for the abstraction of a hydrogen atom from C15 and the subsequent oxidation at C17. In order to understand this binding event in more detail, DHA and 7S-HDHA were modeled into the active site of h15-LOX-2. Both substrates bind in a tail first U-shaped binding mode with their carboxylate groups forming a salt-bridge with R429 on the helix α12. Their hydrophobic tails are buried deep in a hydrophobic pocket created by residues F365, L420, I421, V427, F438, and L607 (Fig. 4), and the reactive pro-S hydrogen of C15 of 7S-HDHA is 2.7 Å from the active site hydroxide-ferric moiety.

This binding mode is consistent with the abstraction of the pro-S hydrogen atom from C15 to produce 7S,17S-diHp-DHA. Parenthetically, the pro-S hydrogen is also abstracted in the formation of 12-HETE, 5-HETE, and 15-HETE by h12-LOX, h5-LOX, and h15-LOX-1, respectively (66–70).

Biological consequences

The above experimental results were performed under conditions different from the cellular milieu; however, if we consider that the in vitro biosynthetic pathways outlined above for 7S,14S-diHDHA and 7S,17S-diHDHA could be viable in in vivo systems and that both molecules are biologically active, then this data opens up the possibility for involvement of new cells types not previously considered in SPM formation. For example, cellular interactions within blood clots are proposed to lead to the synthesis of SPM through the process of transcellular biosynthesis (29, 30); therefore, cell types that contain h5-LOX and h15-LOX-1 may participate in the transcellular biosynthesis of 7S,14S-diHDHA. Also, h15-LOX-1 is expressed at high levels in macrophages (79–81), while h5-LOX is expressed at high levels in neutrophils (82–84), and becaise they are often colocalized at sites of inflammation and thrombosis, these two cell types may be involved in the transcellular biosynthesis of 7S,14S-diHDHA. In addition, macrophages can express both h5-LOX and h15-LOX-1, so in the simplest terms, macrophages may be able to synthesize 7S,14S-diHDHA without participation of other cell types for transcellular biosynthesis. This is especially relevant because we did not observe platelets producing 7S,14S-diHDHA when given 7S-HDHA; therefore, the cellular milieu may affect h12-LOX activity because we observe 7S,14S-diHDHA in vitro. We are currently investigating these biosynthetic pathways in platelets and macrophages in more detail to identify both the pathway and the cell type that make these oxylipins.

Second, if h15-LOX-2 is the primary enzyme involved in the in vivo RvD5 biosynthesis, then the role of h15-LOX-2 in human disease could be larger than expected. It is known that h15-LOX-2 converts the h5-LOX-derived pro-inflammatory oxylipins, 5S-HETE and 5,6-diHETE, into pro-resolving molecules, such as lipoxins, in vitro (85). With the knowledge that h15-LOX-2 also efficiently produces RvD5 from 7S-HDHA, it could be that h15-LOX-2 is important in mediating the switch between inflammation and resolution. For example, neutrophils express both h5-LOX and h15-LOX-2, so it is conceivable that neutrophils produce RvD5 independently, without the need for a transcellular synthesis mechanism. However, it should be noted that RvD5 production has been observed by exposing isolated neutrophils to 17S-HpDHA (44), suggesting that h5-LOX can produce RvD5 in neutrophils. This result is in contrast to our in vitro results and suggests that there may be a factor in the neutrophils, similar to the role of FLAP, which could increase the h5-LOX activity with 17S-HDHA (86). In macrophages, DHA-derived SPM production is affected by subcellular localization of h5-LOX and its interaction with FLAP (58). Nuclear localization of h5-LOX can be altered by signaling of resolvin D1 (7S,8R,17S-triHDHA) through a calcium-mediated kinase pathway (87), suggesting that other DHA-derived SPMs, such as 17S-HDHA, may have similar effects. We are currently investigating this discrepancy further by investigating neutrophils with our selective LOX inhibitors.

With respect to blood coagulation, this work shows that RvD5 has micromolar potency in inhibiting platelet activation, indicating that h15-LOX-2 may also play a role in hemostasis. RvD5 levels are reduced in blood treated with anticoagulants in vitro (88) and RvD5 formation does not occur during initial platelet activation; however, it is produced in later stages of clot progression (88). Given our result that RvD5 reduces platelet activation, the production of RvD5 could be a signal to diminish the clot size. Given that platelets do not produce h15-LOX-2 and thus cannot make RvD5, these results suggest that RvD5 is formed by h15-LOX-2 in macrophages and/or neutrophils, which migrate into the area of late-stage clots and increase their RvD5 production by increasing the h15-LOX-2 expression but not that of h15-LOX-1 (4). We are currently investigating the role of h15-LOX-2 in more detail with our specific/potent h15-LOX-2 inhibitors (48) with the hope of understanding the correct biosynthesis pathway of RvD5 and hence its role in coagulation and atherosclerotic disorders.

CONCLUSIONS

7S,14S-diHDHA is synthesized in vitro by the sequential reactions of h5-LOX and h12-LOX with DHA. However, we have also discovered an alternative biosynthetic pathway for the production of 7S,14S-diHDHA, which involves h15-LOX-1. The alcohol on 7S-HDHA changes the binding position of the oxylipin in the active site, thus altering the product specificity and possibly affecting our understanding of in vivo biosynthetic pathways. It first indicates a possible alternative biosynthetic pathway for 7S,14S-diHDHA in vivo; but more importantly, the result indicates that our knowledge of LOX reactivities with fatty acids may not extend to oxylipins, and therefore further study is needed to determine the exact biosynthetic pathways for each oxylipin, such as lipoxins, protectins, and maresins. Importantly, these results suggest that LOX-products observed during in vivo studies may originate from noncanonical biosynthetic routes involving previously overlooked cell types.

In addition, this result suggests that the biosynthesis of 7S,17S-diHDHA (RvD5) is achieved with h15-LOX-2, and thus its role in human disease may be more important than previously suspected. These results are especially relevant because we have discovered that both 7S,14S-diHDHA and 7S,17S-diHDHA (RvD5) are micromolar anti-aggregation effector molecules that could possibly be synthesized directly from macrophages or neutrophils, respectively, without the need for a transcellular mechanism of biosynthesis, suggesting that both 7S,14S-diHDHA and 7S,17S-diHDHA (RvD5) may be more intimately involved in stopping the aggregation process in clot resolution than previously suspected. Thus, targeting the kinetics of platelet aggregation or clot resolution at sites of inflammation by inhibiting the

biosynthesis of either 7S,14S-diHDHA and 7S,17S-diHDHA (RvD5) may represent a new therapeutic target for future development.

Data availability

All data are contained in the article or the supplemental material. Accession IDs: P18054, h12-LOX; O15296, h15-LOX-2; P09917, h5-LOX; P16050, h15-LOX-1.

REFERENCES

1. Tabas, I., and C. K. Glass. 2013. Anti-inflammatory therapy in chronic disease: challenges and opportunities. *Science.* **339:** 166–172.
2. Serhan, C. N., and N. A. Petasis. 2011. Resolvins and protectins in inflammation resolution. *Chem. Rev.* **111:** 5922–5943.
3. Hultén, L. M., F. J. Olson, H. Aberg, J. Carlsson, L. Karlstrom, J. Borén, B. Fagerberg, and O. Wiklund. 2010. 15-Lipoxygenase-2 is expressed in macrophages in human carotid plaques and regulated by hypoxia-inducible factor-1alpha. *Eur. J. Clin. Invest.* **40:** 11–17.
4. Gertow, K., E. Nobili, L. Folkersen, J. W. Newman, T. L. Pedersen, J. Ekstrand, J. Swedenborg, H. Kuhn, C. E. Wheelock, G. K. Hansson, et al. 2011. 12- and 15-lipoxygenases in human carotid atherosclerotic lesions: associations with cerebrovascular symptoms. *Atherosclerosis.* **215:** 411–416.
5. Danielsson, K. N., E. K. Rydberg, M. Ingelsten, L. M. Akyurek, P. Jirholt, C. Ullstrom, G. B. Forsberg, J. Boren, O. Wiklund, and L. M. Hulten. 2008. 15-Lipoxygenase-2 expression in human macrophages induces chemokine secretion and T cell migration. *Atherosclerosis.* **199:** 34–40.
6. Weaver, J. R., T. R. Holman, Y. Imai, A. Jadhav, V. Kenyon, D. J. Maloney, J. L. Nadler, G. Rai, A. Simeonov, and D. A. Taylor-Fishwick. 2012. Integration of pro-inflammatory cytokines, 12-lipoxygenase and NOX-1 in pancreatic islet beta cell dysfunction. *Mol. Cell. Endocrinol.* **358:** 88–95.
7. Cole, B. K., D. C. Lieb, A. D. Dobrian, and J. L. Nadler. 2013. 12- and 15-lipoxygenases in adipose tissue inflammation. *Prostaglandins Other Lipid Mediat.* **104–105:** 84–92.
8. Mangino, M. J., L. Brounts, B. Harms, and C. Heise. 2006. Lipoxin biosynthesis in inflammatory bowel disease. *Prostaglandins Other Lipid Mediat.* **79:** 84–92.
9. Serhan, C. N., N. Chiang, and T. E. Van Dyke. 2008. Resolving inflammation: dual anti-inflammatory and pro-resolution lipid mediators. *Nat. Rev. Immunol.* **8:** 349–361.
10. Ivanov, I., D. Heydeck, K. Hofheinz, J. Roffeis, V. B. O'Donnell, H. Kuhn, and M. Walther. 2010. Molecular enzymology of lipoxygenases. *Arch. Biochem. Biophys.* **503:** 161–174.
11. Çolakoğlu, M., S. Tuncer, and S. Banerjee. 2018. Emerging cellular functions of the lipid metabolizing enzyme 15-Lipoxygenase-1. *Cell Prolif.* **51:** e12472.
12. Ford-Hutchinson, A. W. 1991. Arachidonate 15-lipoxygenase; characteristics and potential biological significance. *Eicosanoids.* **4:** 65–74.
13. Brash, A. R., W. E. Boeglin, and M. S. Chang. 1997. Discovery of a second 15S-lipoxygenase in humans. *Proc. Natl. Acad. Sci. USA.* **94:** 6148–6152.
14. Jisaka, M., R. B. Kim, W. E. Boeglin, L. B. Nanney, and A. R. Brash. 1997. Molecular cloning and functional expression of a phorbol ester-inducible 8S-lipoxygenase from mouse skin. *J. Biol. Chem.* **272:** 24410–24416.
15. Green, A. R., S. Barbour, T. Horn, J. Carlos, J. A. Raskatov, and T. R. Holman. 2016. Strict Regiospecificity of human epithelial 15-lipoxygenase-2 delineates its transcellular synthesis potential. *Biochemistry.* **55:** 2832–2840.
16. Magnusson, L. U., A. Lundqvist, M. N. Karlsson, K. Skalen, M. Levin, O. Wiklund, J. Boren, and L. M. Hulten. 2012. Arachidonate 15-lipoxygenase type B knockdown leads to reduced lipid accumulation and inflammation in atherosclerosis. *PLoS One.* **7:** e43142.
17. Serhan, C. N., R. Yang, K. Martinod, K. Kasuga, P. S. Pillai, T. F. Porter, S. F. Oh, and M. Spite. 2009. Maresins: novel macrophage mediators with potent antiinflammatory and proresolving actions. *J. Exp. Med.* **206:** 15–23.
18. Freedman, C., A. Tran, B. E. Tourdot, C. Kalyanaraman, S. Perry, M. Holinstat, M. P. Jacobson, and T. R. Holman. Biosynthesis of the maresin intermediate, 13S,14S-epoxy-DHA, by human 15-lipoxygenase and 12-lipoxygenase and its regulation through negative allosteric modulators. *Biochemistry.* Epub ahead of print. May 7, 2020; doi:10.1021/acs.biochem.0c00233.
19. Gu, Z., G. J. Lamont, R. J. Lamont, S. M. Uriarte, H. Wang, and D. A. Scott. 2016. Resolvin D1, resolvin D2 and maresin 1 activate the GSK3beta anti-inflammatory axis in TLR4-engaged human monocytes. *Innate Immun.* **22:** 186–195.
20. Green, A. R., C. Freedman, J. Tena, B. E. Tourdot, B. Liu, M. Holinstat, and T. R. Holman. 2018. 5 S,15 S-dihydroperoxyeicosatetraenoic acid (5,15-diHpETE) as a lipoxin intermediate: reactivity and kinetics with human leukocyte 5-lipoxygenase, platelet 12-lipoxygenase, and reticulocyte 15-lipoxygenase-1. *Biochemistry.* **57:** 6726–6734.
21. Edenius, C., J. Haeggstrom, and J. A. Lindgren. 1988. Transcellular conversion of endogenous arachidonic acid to lipoxins in mixed human platelet-granulocyte suspensions. *Biochem. Biophys. Res. Commun.* **157:** 801–807.
22. Sheppard, K. A., S. M. Greenberg, C. D. Funk, M. Romano, and C. N. Serhan. 1992. Lipoxin generation by human megakaryocyte-induced 12-lipoxygenase. *Biochim. Biophys. Acta.* **1133:** 223–234.
23. Serhan, C. N., S. Hong, K. Gronert, S. P. Colgan, P. R. Devchand, G. Mirick, and R. L. Moussignac. 2002. Resolvins: a family of bioactive products of omega-3 fatty acid transformation circuits initiated by aspirin treatment that counter proinflammation signals. *J. Exp. Med.* **196:** 1025–1037.
24. Dalli, J., R. A. Colas, and C. N. Serhan. 2013. Novel n-3 immunoresolvents: structures and actions. *Sci. Rep.* **3:** 1940–1953.
25. Chiang, N., G. Fredman, F. Backhed, S. F. Oh, T. Vickery, B. A. Schmidt, and C. N. Serhan. 2012. Infection regulates pro-resolving mediators that lower antibiotic requirements. *Nature.* **484:** 524–528.
26. Giera, M., A. Ioan-Facsinay, R. Toes, F. Gao, J. Dalli, A. M. Deelder, C. N. Serhan, and O. A. Mayboroda. 2012. Lipid and lipid mediator profiling of human synovial fluid in rheumatoid arthritis patients by means of LC-MS/MS. *Biochim. Biophys. Acta.* **1821:** 1415–1424.
27. Hong, S., K. Gronert, P. R. Devchand, R. L. Moussignac, and C. N. Serhan. 2003. Novel docosatrienes and 17S-resolvins generated from docosahexaenoic acid in murine brain, human blood, and glial cells. Autacoids in anti-inflammation. *J. Biol. Chem.* **278:** 14677–14687.
28. Serhan, C. N., K. Gotlinger, S. Hong, Y. Lu, J. Siegelman, T. Baer, R. Yang, S. P. Colgan, and N. A. Petasis. 2006. Anti-inflammatory actions of neuroprotectin D1/protectin D1 and its natural stereoisomers: assignments of dihydroxy-containing docosatrienes. *J. Immunol.* **176:** 1848–1859.
29. Serhan, C. N., and K. A. Sheppard. 1990. Lipoxin formation during human neutrophil-platelet interactions. Evidence for the transformation of leukotriene A4 by platelet 12-lipoxygenase in vitro. *J. Clin. Invest.* **85:** 772–780.
30. Deng, B., C. W. Wang, H. H. Arnardottir, Y. Li, C. Y. Cheng, J. Dalli, and C. N. Serhan. 2014. Maresin biosynthesis and identification of maresin 2, a new anti-inflammatory and pro-resolving mediator from human macrophages. *PLoS One.* **9:** e102362.
31. Sala, A., T. Testa, and G. Folco. 1996. Leukotriene A4, and not leukotriene B4, is the main 5-lipoxygenase metabolite released by bovine leukocytes. *FEBS Lett.* **388:** 94–98.
32. Barden, A. E., S. Shinde, V. Burke, I. B. Puddey, L. J. Beilin, A. B. Irish, G. F. Watts, and T. A. Mori. 2018. The effect of n-3 fatty acids and coenzyme Q10 supplementation on neutrophil leukotrienes, mediators of inflammation resolution and myeloperoxidase in chronic kidney disease. *Prostaglandins Other Lipid Mediat.* **136:** 1–8.
33. Norris, P. C., and C. N. Serhan. 2018. Metabololipidomic profiling of functional immunoresolvent clusters and eicosanoids in mammalian tissues. *Biochem. Biophys. Res. Commun.* **504:** 553–561.
34. Serhan, C. N., J. Dalli, S. Karamnov, A. Choi, C. K. Park, Z. Z. Xu, R. R. Ji, M. Zhu, and N. A. Petasis. 2012. Macrophage proresolving mediator maresin 1 stimulates tissue regeneration and controls pain. *FASEB J.* **26:** 1755–1765.
35. Deschamps, J. D., V. A. Kenyon, and T. R. Holman. 2006. Baicalein is a potent in vitro inhibitor against both reticulocyte 15-human and platelet 12-human lipoxygenases. *Bioorg. Med. Chem.* **14:** 4295–4301.
36. Kutzner, L., K. Goloshchapova, D. Heydeck, S. Stehling, H. Kuhn, and N. H. Schebb. 2017. Mammalian ALOX15 orthologs exhibit pronounced dual positional specificity with docosahexaenoic acid. *Biochim. Biophys. Acta Mol. Cell Biol. Lipids.* **1862:** 666–675.
37. Lee, T. H., J. M. Mencia-Huerta, C. Shih, E. J. Corey, R. A. Lewis, and K. F. Austen. 1984. Effects of exogenous arachidonic, eicosapentaenoic, and docosahexaenoic acids on the generation of

5-lipoxygenase pathway products by ionophore-activated human neutrophils. *J. Clin. Invest.* **74:** 1922–1933.
38. Smyrniotis, C. J., S. R. Barbour, Z. Xia, M. S. Hixon, and T. R. Holman. 2014. ATP allosterically activates the human 5-lipoxygenase molecular mechanism of arachidonic acid and 5(S)-hydroperoxy-6(E),8(Z),11(Z),14(Z)-eicosatetraenoic acid. *Biochemistry.* **53:** 4407–4419.
39. Adel, S., F. Karst, A. Gonzalez-Lafont, M. Pekarova, P. Saura, L. Masgrau, J. M. Lluch, S. Stehling, T. Horn, H. Kuhn, et al. 2016. Evolutionary alteration of ALOX15 specificity optimizes the biosynthesis of antiinflammatory and proresolving lipoxins. *Proc. Natl. Acad. Sci. USA.* **113:** E4266–E4275.
40. 2016. Correction for Adel et al., Evolutionary alteration of ALOX15 specificity optimizes the biosynthesis of antiinflammatory and proresolving lipoxins. *Proc. Natl. Acad. Sci. USA.* **113:** E8006.
41. Abrial, C., S. Grassin-Delyle, H. Salvator, M. Brollo, E. Naline, and P. Devillier. 2015. 15-Lipoxygenases regulate the production of chemokines in human lung macrophages. *Br. J. Pharmacol.* **172:** 4319–4330.
42. Snodgrass, R. G., E. Zezina, D. Namgaladze, S. Gupta, C. Angioni, G. Geisslinger, D. Lutjohann, and B. Brune. 2018. A Novel Function for 15-Lipoxygenases in Cholesterol Homeostasis and CCL17 Production in Human Macrophages. *Front. Immunol.* **9:** 1906–1932.
43. Werz, O., J. Gerstmeier, S. Libreros, X. De la Rosa, M. Werner, P. C. Norris, N. Chiang, and C. N. Serhan. 2018. Human macrophages differentially produce specific resolvin or leukotriene signals that depend on bacterial pathogenicity. *Nat. Commun.* **9:** 59.
44. Archambault, A. S., C. Turcotte, C. Martin, V. Provost, M. C. Larose, C. Laprise, J. Chakir, E. Bissonnette, M. Laviolette, Y. Bosse, et al. 2018. Comparison of eight 15-lipoxygenase (LO) inhibitors on the biosynthesis of 15-LO metabolites by human neutrophils and eosinophils. *PLoS One.* **13:** e0202424.
45. Maas, R. L., J. Turk, J. A. Oates, and A. R. Brash. 1982. Formation of a novel dihydroxy acid from arachidonic acid by lipoxygenase-catalyzed double oxygenation in rat mononuclear cells and human leukocytes. *J. Biol. Chem.* **257:** 7056–7067.
46. Amagata, T., S. Whitman, T. A. Johnson, C. C. Stessman, C. P. Loo, E. Lobkovsky, J. Clardy, P. Crews, and T. R. Holman. 2003. Exploring sponge-derived terpenoids for their potency and selectivity against 12-human, 15-human, and 15-soybean lipoxygenases. *J. Nat. Prod.* **66:** 230–235.
47. Robinson, S. J., E. K. Hoobler, M. Riener, S. T. Loveridge, K. Tenney, F. A. Valeriote, T. R. Holman, and P. Crews. 2009. Using enzyme assays to evaluate the structure and bioactivity of sponge-derived meroterpenes. *J. Nat. Prod.* **72:** 1857–1863.
48. Jameson, J. B., A. Kantz, L. Schultz, C. Kalyanaraman, M. P. Jacobson, D. J. Maloney, A. Jadhav, A. Simeonov, and T. R. Holman. 2014. A high throughput screen identifies potent and selective inhibitors to human epithelial 15-lipoxygenase-2. *PLoS One.* **9:** e104094.
49. Butovich, I. A. 2006. A one-step method of 10,17-dihydro(pero)xydocosahexa-4Z,7Z,11E,13Z,15E,19Z-enoic acid synthesis by soybean lipoxygenase. *J. Lipid Res.* **47:** 854–863.
50. Fitzgerald, J. C. R., M. Shinohara, D. Dalli, and C. Serhan. 2014. Lipid Mediator Metabololipidomics LC-MS-MS Spectra Book 2014. Available from: http://serhanlab.bwh.harvard.edu/wp-content/uploads/2019/05/UPDATED-2019-Spectra-Book.pdf
51. Wecksler, A. T., C. Jacquot, W. A. van der Donk, and T. R. Holman. 2009. Mechanistic investigations of human reticulocyte 15- and platelet 12-lipoxygenases with arachidonic acid. *Biochemistry.* **48:** 6259–6267.
52. Segraves, E. N., and T. R. Holman. 2003. Kinetic investigations of the rate-limiting step in human 12- and 15-lipoxygenase. *Biochemistry.* **42:** 5236–5243.
53. Aveldaño, M. I., and H. Sprecher. 1983. Synthesis of hydroxy fatty acids from 4, 7, 10, 13, 16, 19-[1–14C] docosahexaenoic acid by human platelets. *J. Biol. Chem.* **258:** 9339–9343.
54. Guichardant, M., and M. Lagarde. 1985. Studies on platelet lipoxygenase specificity towards icosapolyenoic and docosapolyenoic acids. *Biochim. Biophys. Acta.* **836:** 210–214.
55. Van Os, C. P., G. P. Rijke-Schilder, H. Van Halbeek, J. Verhagen, and J. F. Vliegenthart. 1981. Double dioxygenation of arachidonic acid by soybean lipoxygenase-1. Kinetics and regio-stereo specificities of the reaction steps. *Biochim. Biophys. Acta.* **663:** 177–193.
56. Cipollina, C., S. R. Salvatore, M. F. Muldoon, B. A. Freeman, and F. J. Schopfer. 2014. Generation and dietary modulation of anti-inflammatory electrophilic omega-3 fatty acid derivatives. *PLoS One.* **9:** e94836.
57. Koltsida, O., S. Karamnov, K. Pyrillou, T. Vickery, A. D. Chairakaki, C. Tamvakopoulos, P. Sideras, C. N. Serhan, and E. Andreakos. 2013. Toll-like receptor 7 stimulates production of specialized pro-resolving lipid mediators and promotes resolution of airway inflammation. *EMBO Mol. Med.* **5:** 762–775.
58. Werner, M., P. M. Jordan, E. Romp, A. Czapka, Z. Rao, C. Kretzer, A. Koeberle, U. Garscha, S. Pace, H. E. Claesson, et al. 2019. Targeting biosynthetic networks of the proinflammatory and proresolving lipid metabolome. *FASEB J.* **33:** 6140–6153.
59. Northrop, D. B. 1998. On the meaning of Km and V/K in enzyme kinetics. *J. Chem. Educ.* **75:** 1153–1157.
60. Chen, P., B. Fenet, S. Michaud, N. Tomczyk, E. Vericel, M. Lagarde, and M. Guichardant. 2009. Full characterization of PDX, a neuroprotectin/protectin D1 isomer, which inhibits blood platelet aggregation. *FEBS Lett.* **583:** 3478–3484.
61. Aursnes, M., J. E. Tungen, A. Vik, R. Colas, C. Y. Cheng, J. Dalli, C. N. Serhan, and T. V. Hansen. 2014. Total synthesis of the lipid mediator PD1n-3 DPA: configurational assignments and anti-inflammatory and pro-resolving actions. *J. Nat. Prod.* **77:** 910–916.
62. Tungen, J. E., M. Aursnes, A. Vik, S. Ramon, R. A. Colas, J. Dalli, C. N. Serhan, and T. V. Hansen. 2014. Synthesis and anti-inflammatory and pro-resolving activities of 22-OH-PD1, a monohydroxylated metabolite of protectin D1. *J. Nat. Prod.* **77:** 2241–2247.
63. Balas, L., M. Guichardant, T. Durand, and M. Lagarde. 2014. Confusion between protectin D1 (PD1) and its isomer protectin DX (PDX). An overview on the dihydroxy-docosatrienes described to date. *Biochimie.* **99:** 1–7.
64. Friesner, R. A., J. L. Banks, R. B. Murphy, T. A. Halgren, J. J. Klicic, D. T. Mainz, M. P. Repasky, E. H. Knoll, M. Shelley, J. K. Perry, et al. 2004. Glide: a new approach for rapid, accurate docking and scoring. 1. Method and assessment of docking accuracy. *J. Med. Chem.* **47:** 1739–1749.
65. Gan, Q-F., M. F. Browner, D. L. Sloane, and E. Sigal. 1996. Defining the arachidonic acid binding site of human 15-lipoxygenase: molecular modeling and mutagenesis. *J. Biol. Chem.* **271:** 25412–25418.
66. Suardíaz, R., P. G. Jambrina, L. Masgrau, A. Gonzalez-Lafont, E. Rosta, and J. M. Lluch. 2016. Understanding the mechanism of the hydrogen abstraction from arachidonic acid catalyzed by the human enzyme 15-lipoxygenase-2. A quantum mechanics/molecular mechanics free energy simulation. *J. Chem. Theory Comput.* **12:** 2079–2090.
67. Maas, R. L., C. D. Ingram, D. F. Taber, J. A. Oates, and A. R. Brash. 1982. Stereospecific removal of the DR hydrogen atom at the 10-carbon of arachidonic acid in the biosynthesis of leukotriene A4 by human leukocytes. *J. Biol. Chem.* **257:** 13515–13519.
68. Brash, A. R. 1999. Lipoxygenases: occurrence, functions, catalysis, and acquisition of substrate. *J. Biol. Chem.* **274:** 23679–23682.
69. Newcomer, M. E., and A. R. Brash. 2015. The structural basis for specificity in lipoxygenase catalysis. *Protein Sci.* **24:** 298–309.
70. Hamberg, M., and B. Samuelsson. 1967. On the specificity of the oxygenation of unsaturated fatty acids catalyzed by soybean lipoxidase. *J. Biol. Chem.* **242:** 5329–5335.
71. Yeung, J., M. Hawley, and M. Holinstat. 2017. The expansive role of oxylipins on platelet biology. *J. Mol. Med. (Berl.).* **95:** 575–588.
72. Tourdot, B. E., R. Adili, Z. R. Isingizwe, M. Ebrahem, J. C. Freedman, T. R. Holman, and M. Holinstat. 2017. 12-HETrE inhibits platelet reactivity and thrombosis in part through the prostacyclin receptor. *Blood Adv.* **1:** 1124–1131.
73. Ikei, K. N., J. Yeung, P. L. Apopa, J. Ceja, J. Vesci, T. R. Holman, and M. Holinstat. 2012. Investigations of human platelet-type 12-lipoxygenase: role of lipoxygenase products in platelet activation. *J. Lipid Res.* **53:** 2546–2559.
74. Yeung, J., B. E. Tourdot, R. Adili, A. R. Green, C. J. Freedman, P. Fernandez-Perez, J. Yu, T. R. Holman, and M. Holinstat. 2016. 12(S)-HETrE, a 12-lipoxygenase oxylipin of dihomo-gamma-linolenic acid, inhibits thrombosis via Galphas signaling in platelets. *Arterioscler. Thromb. Vasc. Biol.* **36:** 2068–2077.
75. Horitani, M., A. R. Offenbacher, C. A. Carr, T. Yu, V. Hoeke, G. E. Cutsail 3rd, S. Hammes-Schiffer, J. P. Klinman, and B. M. Hoffman. 2017. (13)C ENDOR spectroscopy of lipoxygenase-substrate complexes reveals the structural basis for C-H activation by tunneling. *J. Am. Chem. Soc.* **139:** 1984–1997.
76. Joshi, N., E. K. Hoobler, S. Perry, G. Diaz, B. Fox, and T. R. Holman. 2013. Kinetic and structural investigations into the allosteric and pH effect on the substrate specificity of human epithelial 15-lipoxygenase-2. *Biochemistry.* **52:** 8026–8035.

77. Sloane, D. L., R. Leung, C. S. Craik, and E. Sigal. 1991. A Primary determinant for Lipoxygenase positional specificity. *Nature.* **354:** 149–152.
78. Kuhn, H. 2000. Structural basis for the positional specificity of lipoxygenases. *Prostaglandins Other Lipid Mediat.* **62:** 255–270.
79. Ylä-Herttuala, S., M. E. Rosenfeld, S. Parthasarathy, C. K. Glass, E. Sigal, J. L. Witztum, and D. Steinberg. 1990. Colocalization of 15-lipoxygenase mRNA and protein with epitopes of oxidized low density lipoprotein in macrophage-rich areas of atherosclerotic lesions. *Proc. Natl. Acad. Sci. USA.* **87:** 6959–6963.
80. Kühn, H., J. Belkner, S. Zaiss, T. Fahrenklemper, and S. Wohlfeil. 1994. Involvement of 15-lipoxygenase in early stages of atherogenesis. *J. Exp. Med.* **179:** 1903–1911.
81. Folcik, V. A., R. A. Nivar-Aristy, L. P. Krajewski, and M. K. Cathcart. 1995. Lipoxygenase contributes to the oxidation of lipids in human atherosclerotic plaques. *J. Clin. Invest.* **96:** 504–510.
82. Woods, J. W., J. F. Evans, D. Ethier, S. Scott, P. J. Vickers, L. Hearn, J. A. Heibein, S. Charleson, and I. I. Singer. 1993. 5-lipoxygenase and 5-lipoxygenase-activating protein are localized in the nuclear envelope of activated human leukocytes. *J. Exp. Med.* **178:** 1935–1946.
83. Rouzer, C. A., T. Matsumoto, and B. Samuelsson. 1986. Single protein from human leukocytes possesses 5-lipoxygenase and leukotriene A4 synthase activities. *Proc. Natl. Acad. Sci. USA.* **83:** 857–861.
84. Ueda, N., S. Kaneko, T. Yoshimoto, and S. Yamamoto. 1986. Purification of arachidonate 5-lipoxygenase from porcine leukocytes and its reactivity with hydroperoxyeicosatetraenoic acids. *J. Biol. Chem.* **261:** 7982–7988.
85. Ringholz, F. C., P. J. Buchanan, D. T. Clarke, R. G. Millar, M. McDermott, B. Linnane, B. J. Harvey, P. McNally, and V. Urbach. 2014. Reduced 15-lipoxygenase 2 and lipoxin A4/leukotriene B4 ratio in children with cystic fibrosis. *Eur. Respir. J.* **44:** 394–404.
86. Peters-Golden, M., and T. G. Brock. 2003. 5-lipoxygenase and FLAP. *Prostaglandins Leukot. Essent. Fatty Acids.* **69:** 99–109.
87. Fredman, G., L. Ozcan, S. Spolitu, J. Hellmann, M. Spite, J. Backs, and I. Tabas. 2014. Resolvin D1 limits 5-lipoxygenase nuclear localization and leukotriene B4 synthesis by inhibiting a calcium-activated kinase pathway. *Proc. Natl. Acad. Sci. USA.* **111:** 14530–14535.
88. Norris, P. C., S. Libreros, N. Chiang, and C. N. Serhan. 2017. A cluster of immunoresolvents links coagulation to innate host defense in human blood. *Sci. Signal.* **10:** eaan1471.